Clim Dyn (2017) 49:1077–1105
DOI 10.1007/s00382-016-3234-0

Observed variability in the upper layers at the Equator, 90°E in the Indian Ocean during 2001–2008, 1: zonal currents

R. R. Rao[1] · T. Horii[2] · Y. Masumoto[2,3] · K. Mizuno[2]

Received: 6 May 2015 / Accepted: 8 June 2016 / Published online: 20 June 2016

Abstract The observed variability of zonal currents (ZC) at the Equator, 90°E shows a strong seasonal cycle in the near-surface 40–350 m water column with periodic east–west reversals most pronounced at semiannual frequency. Superposed on this, a strong intraseasonal variability of 30–90 day periodicity is also prominently seen in the near-surface layer (40–80 m) almost throughout the year with the only exception of February–March. An eastward flowing equatorial undercurrent (EUC) is present in the depth range of 80–160 m during March–April and October–November. The observed intraseasonal variability in the near-surface layer is primarily determined by the equatorial zonal westerly wind bursts (WWBs) through local frictional coupling between the zonal flow in the surface layer and surface zonal winds and shows large interannual variability. The eastward flowing EUC maintained by the ZPG set up by the east–west slope of the thermocline remotely controlled by the zonal wind (ZW) and zonally propagating wave fields also shows significant interannual variability. This observed variability on interannual time scales appears to be controlled by the corresponding variability in the alongshore winds off the Somalia coast during the preceding boreal winter, the ZW field along the equator, and the associated zonally propagating Kelvin and Rossby waves. The salinity induced vertical stratification observed in the near-surface layer through barrier layer thickness (BLT) effects also shows a significant influence on the ZC field on intraseasonal time scale. Interestingly, among all the 8 years (2001–2008), relatively weaker annual cycle is seen in both ZC in the 40–350 m water column and boreal spring sea surface temperature (SST) only during 2001 and 2008 along the equator caused through propagating wave dynamics.

Keywords Indian Ocean · Equatorial zonal currents · Equatorial undercurrent · Intraseasonal variability · Westerly wind bursts · Interannual variability · Barrier layer thickness · Sea surface temperature

1 Introduction

In the tropics, the Indian Ocean stands out quite unique when compared to the Atlantic and Pacific Oceans as it is strongly coupled with the seasonally reversing monsoons and shows large variability both on spatial and temporal scales. Any excessive or deficient rainfall associated with the monsoons and the meteorological disturbances have a huge impact on the lives of a third of the global population. In the context of the regional monsoon climate, the issues of particular interest are the onset and active-break cycles of the monsoons, intraseasonal Madden–Julian Oscillations (MJO), tropical cyclones, interannual variations associated with ENSO and the Indian Ocean Dipole (IOD). In recent years, the attention of the international scientific community has shifted to the least explored and understood tropical Indian Ocean (TIO) resulting in several new major observational initiatives through international collaboration

This paper is a contribution to the special issue on Ocean estimation from an ensemble of global ocean reanalyses, consisting of papers from the Ocean Reanalyses Intercomparsion Project (ORAIP), coordinated by CLIVAR-GSOP and GODAE OceanView. The special issue also contains specific studies using single reanalysis systems.

✉ R. R. Rao
rokkamrr@yahoo.com

[1] ICMPO, IITM, Pune, India

[2] JAMSTEC, Yokosuka, Japan

[3] University of Tokyo, Tokyo, Japan

and by the countries surrounding (Hood et al. 2008). Under the aegis of Research Moored Array for African–Asian–Australian Monsoon Analysis and Prediction (RAMA)—deployment of sustained moored buoy array has been taken up to improve our understanding of large scale ocean dynamics, ocean–atmosphere interactions, and climate variability in the Indian Ocean region (McPhaden et al. 2009).

The TIO is the smallest of the tropical ocean basins and is unique with its land locking on three sides and opening only to the Indonesian Throughflow and the southern ocean. The surface wind field is also unique with its distinct seasonal reversal and so is the time dependent near-surface circulation. Historically, oceanographers have paid much attention to the western equatorial Indian Ocean (EIO) and the western Arabian Sea where the monsoon winds are well known to be quite strong resulting in a strong western boundary current—the Somalia Current. All the available historic in situ data have provided a basic description of the observed seasonal cycle and the probable governing mechanisms but could not resolve the observed small scale variability due to lack of high resolution measurements both in space and time. The advent of satellite era has opened up new dimensions by providing repeat synoptic views of the global ocean to explore the high frequency variability that is found to be more pronounced in the warmer regions of the tropical basins. In addition, the new in situ observing technologies such as ARGO profiling floats, drifting buoys, moored current meters, sea gliders and ADCP moorings are supplementing our ability to describe and understand the ocean circulation and its influence on climate on finer spatio-temporal scales. One of the least known facets of the TIO is the nature of the variability in the circulation below the surface. To address this important issue, JAMSTEC has thoughtfully pioneered in the deployment of upward looking ADCP at about 400 m depth at the Equator, 90°E in the core of the warm pool region of the EIO and the time series data are being collected uninterruptedly since 14 November, 2000 coinciding with the RAMA observational initiative. This data set is the longest record ever collected at any single stationary location in the TIO and hence provides a great opportunity for a comprehensive description and understanding of the flow patterns and model validations in the upper layers of the eastern EIO. Before we present our analysis of this data set, our current understanding of the processes in the EIO is briefly reviewed.

2 Background observational and modeling framework

2.1 Seasonal variability

In the Indian Ocean, at the surface along the equator, a narrow jet-like current popularly known as Wyrtki Jet (WJ) flows eastward at high speed during both the transition periods between the two monsoons. The formation of this jet is accompanied by thermocline uplifting at the western origin of the jet and by sinking at its eastern terminal resulting in a gradient of 20 cm in the sea level. This demonstrates that a time variable current can have profound effect in changing the mass structure of the EIO (Wyrtki 1973). The analysis of nearly 2 years (January, 1973–September, 1974) of weekly wind, current and temperature profiles to 300 m depth from Gan Island (0°41′S, 73°10′E) in the central EIO by Knox (1976) shows an eastward jet which appears at both the boreal spring and boreal fall monsoon transitions, driven by strong eastward winds. The jet is almost as strong at the depth of the thermocline as at the surface, and the ZCs at both the depths are well correlated with the local wind stress at essentially zero lag. A purely local balance of forces fails to account for the observed zonal acceleration; non-local effects, mainly the time dependent ZPG, are also found to be important. An eastward flowing EUC beneath a westward surface flow is forced in only one of the 2 years, and this is consistent with certain differences in the surface wind field seen in these 2 years. O'Brien and Hurlburt (1974) offered a simple analytical theory to numerically simulate Wyrtki's observations on the equatorial jet and the east–west tilt of the pycnocline. An equatorial transect made during December 1976–January 1977, has revealed large ZPG due to the presence of large volume of anomalous saline waters east of Maldive Islands transported by the equatorial jets (Eriksen 1979). In a modeling study, Cane (1980) argued that for the westerly and meridional winds the response of equatorial currents is predominantly local and rapid. The current reversals observed at the Gan Island are most likely due to changes in the local winds. The winds at the Gan Island are predominantly westerly, resulting in downwelling at the equator. The eastward momentum put in by the wind at the surface is transported downward giving subsurface eastward flow. With persistent easterlies as seen in the Atlantic and Pacific, there is an eastward flowing EUC driven by the eastward ZPG force. He suggested that the EUC that is observed in the EIO in the early boreal spring is driven by the eastward ZPG. This ZPG is a non-local transient feature generated by the zonal readjustment of mass induced by the relaxation of winds at the preceding boreal fall monsoon transition. This idea is consistent with the presence of the EUC in 1973 and its absence in 1974.

From the Gan Island data, McPhaden (1982) showed that the zonal mean currents are eastward from the surface down to 200 m indicating that non-linearity is important in the mean zonal momentum balance in the thermocline. The amplitude and phase of the semiannual variability below the mixed layer suggests that there is a net downward propagation of energy in the form of equatorial Kelvin

and non-dispersive Rossby waves. The analysis of moored records of zonal velocity in the western EIO (April, 1979–June, 1980) has shown strong semiannual period over a 500 m water column in the vertical and with a upward phase propagation in the presence of zonally propagating Kelvin and Rossby waves (Luyten and Roemmich 1982). Gent et al. (1983) have also concluded that in the upper western EIO, the direct observations (April, 1979–June, 1980) can be accounted for as a directly forced response to the semiannual component of the near-equatorial ZWs. Based on observational analysis of historic data, Reverdin (1987) has reported that along the equator, near the surface and below the thermocline, the observations indicate an intense variability of the currents, primarily at the semiannual frequency. In the thermocline, presence of the EUC during March–April is the dominant feature. At the semiannual period, different isotherms oscillate in phase in the upper western EIO and upward phase propagation is present in the east. The surface equatorial currents strongly depend on the mixed layer depth and the currents in the thermocline are controlled by mixing (Reverdin 1987). Molinari et al. (1990) have analyzed all the available historic trajectories of satellite tracking drifting buoys and ship drift vectors and found that both of these representations of the equatorial jets are similar in direction and amplitude in the central EIO. Their amplitudes and phases of the annual and semiannual modes are also similar in the EIO.

In a model study, Jensen (1993) has found that the equatorial surface jets are associated with intense flow in the opposite direction below the thermocline. The deep semiannual currents change direction during the year, as observed by Luyten and Roemmich (1982). In agreement with observations, the phase propagation was westward and upward. The second baroclinic mode, long Kelvin and Rossby waves are dominant in the equatorial region. They propagate with speeds that allow an equatorial Kelvin wave to cross the EIO in 1.5 months, and reflect part of its energy into a westward propagating Rossby wave, which returns to the western boundary after 4.5 months. The strong response of the EIO to semiannual forcing can be explained in terms of a resonant basin mode, which is a combination of Kelvin and equatorial Rossby waves (Cane and Moore 1981). For semiannual forcing, resonance for an equatorial Kelvin wave speed close to 1.4 m/s is found corresponding to the equatorial Kelvin wave speed for the second baroclinic mode. In an Ocean General Circulation Model (OGCM) simulation, Anderson and Carrington (1993) have shown that equatorial ZC differences at the surface between experiments using UKMO and ECMWF wind stress forcings can be as large as 80 cm/s, comparable to the magnitude of interannual variations.

Based on 51 zonal equatorial transects during 1962–1988, Bubnov (1994) has shown that under prevailing westerly winds, a westerly ZPG dominates in the topmost 100 m water column during the course of an year. The only exception to this is during February–March, when the ZPG acquires an easterly direction. The seasonal cycle of ZPG shows a distinct semiannual mode, with minima in February–March and August and maxima in May and October–December. The ZPG in the near-surface layer changes in phase with the surface ZW stress. Analysis of zonal ship drifts along a meridional transect between Sri Lanka and the equator by Schott et al. (1994) has shown large semiannual (annual) amplitude near the equator (Sri Lankan coast) that decreases rapidly with latitude. Shenoi et al. (1999) have analyzed the trajectories of 412 satellite-tracking drifting buoys deployed in the TIO and have shown that in the equatorial region, in general, the surface flows are eastward, except during July–August, when a narrow westward flow appears at the equator. The eastward WJs that appeared during April–May and again in November are branched near 90°E; a major branch turned southward along the west coast of Sumatra and the other branch turned northward which contributes to the coastal current along the eastern rim of the Bay of Bengal. Based on an observational analysis of the direct current measurements made from a meridional moored array of ADCPs deployed south of Sri Lanka (July 1993–September, 1994), Reppin et al. (1999) have found that the semiannual WJs have shown strong seasonal asymmetry, reaching a monthly eastward transport of 35 Sv in November 1993, but just 5 Sv in May 1994 which was an IOD year. The EUC was stronger during March–April, 1994 in comparison with that of during August–September, 1994. They have concluded that the observed interannual variability of the WJ in their measurements and in the ship drift data appears to be related to the variability of the ZWs and Southern Oscillation Index. In a model simulation, Han et al. (1999) have shown that the direct wind forcing is the dominant mechanism of the WJs, accounting for 81 % variance of their amplitude when there is a mixed layer. Reflected Rossby waves, resonance, and mixed layer shear are all necessary to produce jets with realistic structure and strength. Precipitation during the boreal summer and boreal fall considerably strengthens the boreal fall WJ in the eastern region by thinning the mixed layer. Nagura and McPhaden (2010a) have examined seasonal dynamics of Wyrtki jets. They found that the zonal currents propagate westward along the equator at semiannual periods with an average speed of −1.5 m/s. This propagation speed is three times faster than the propagation speed of the dominant wave mode in model zonal velocity, namely the first meridional, second baroclinic mode Rossby wave. We interpret this result in terms of a superposition of Rossby waves on a wind-forced jet, with the jet stronger than the waves by a factor of 2.

2.2 Interannual variability

A major regional climatic signal Indian Ocean Dipole (IOD) was discovered in the atmosphere–ocean coupled system of the TIO that has large impact on the some of the surrounding countries (Saji et al. 1999). Vinayachandran et al. (1999) have reported unusual westward surface ZW anomalies in the EIO during the IOD year 1994. The eastward WJs were weak and consequently the sea level in the EIO was unusually low, the thermocline and the mixed layer were shallow, and the subsurface flow remained eastward throughout the year. Cooler SST anomalies in the eastern EIO were enhanced by the upwelling-favourable winds along the west coast of Indonesia. Anomalous patterns in the observed near-surface thermohaline structure and circulation in association with the IOD are also noticed in the TIO (Webster et al. 1999; Grodsky et al. 2001; Rao et al. 2002; Rao and Behera 2005; Thompson et al. 2006; Horii et al. 2008; Vinayachandran et al. 2002, 2009 and the references therein). Grodsky et al. (2001) performed the most comprehensive analysis to date, using reanalysis winds, altimeter data and ship drift measurements for the period 1993–2000. They have found that the ZPG and ZW stress were nearly in balance along the equator and the interannual variability in these terms was associated with weakened Wyrtki jets during the IOD events of 1994 and 1997.

Somayajulu et al. (2006) have studied the observed interannual variability of the Equatorial Jets in the Indian Ocean utilising the merged altimetry data set for the years 1997-2005. Nagura and McPhaden (2008) have examined the depth integrated zonal momentum balance for the period October 2004–September 2006 in the central EIO. They have found that 1- to 2-year record length mean balances are approximately linear and steady state. Monthly to seasonal time scale variations are also governed by linear dynamics, with imbalances between the ZPG force and surface ZW stress leading to zonal mass transport variations along the equator. Interannual variations in zonal transports along the equator associated with the IOD events in 1994 and 2006 are likewise consistent with linear dynamics. Analysis of nearly 6 years ADCP data set (January, 2001–November, 2006) collected at the same location of the present study by Iskandar et al. (2009) has focused on the occurrence of EUC in the depth range of 90–170 m during both boreal winter and boreal summer. During boreal winter, the generation of eastward ZPG that drives an eastward flow in the thermocline, is caused primarily by upwelling equatorial Kelvin waves excited by prevailing easterly winds. On the other hand, the downwelling Rossby waves generated by the reflection of the boreal spring downwelling Kelvin waves in the eastern boundary, as well as the upwelling equatorial Kelvin waves excited by prevailing easterly winds, create an oceanic state that favours the generation of the eastward ZPG during boreal summer. This EUC shows significant interannual variations during boreal summer; it was absent during 2003, but it was anomalously strong during the IOD year 2006. Nagura and McPhaden (2010b) have shown that surface zonal velocity on the equator tends to lead zonal wind stress by about 1 month on interannual time scales. This phasing occurs because velocity anomalies reverse before the wind anomalies reverse during the decay of IOD events. The model simulations indicate that this reversal of velocity earlier than winds is caused by reflected Rossby waves radiating from the eastern boundary. In a recent study, Rao et al. (2010) have shown large interannual variability in the eastward propagating Kelvin waves during boreal fall in the EIO that has potential impact on the ZC field. Zeng et al. (2012) have compared ADCP data collected along the equator in the Indian Ocean during May 2010 and April 2011.

2.3 Intraseasonal variability

South of Sri Lanka, the origin of intraseasonal variability (ISV) in the near-surface circulation on time scales of 30–50 days has been hypothesized by Sengupta et al. (2001a) due to amplification of hydrodynamic instability forced by the westward propagating Rossby waves radiated from the eastern boundary of the Bay of Bengal through a modeling study. The summer monsoon ISV also shows coherent patterns meridionally flipping between the northern Bay of Bengal—South China Sea and the eastern EIO with episodes of active and suppressed atmospheric convection (Sengupta et al. 2001b). The variability associated with this convection modulates the WWBs in the EIO during the summer monsoon season.

The model simulation by Han et al. (2001) suggests that the observed 40–60 day surface ZCs are primarily forced by the surface ZW field associated with the MJO which also peaks at 40–60 days. However, the strongest spectral peak in the ZC flow occurs at 90 day period which is also seen in the observed satellite measured sea level data. They attribute this to the preferential excitation of Kelvin and Rossby waves by the lower frequency intraseasonal winds and from the enhancement by Rossby waves reflected from the eastern boundary. The importance of equatorial eastern and western boundary reflections of both Kelvin and Rossby waves was highlighted by Le Blanc and Boulanger (2001). The reflected Kelvin waves strongly influence Rossby wave variability near the western boundary as far as 60°E. Reflected Rossby waves in turn, influence the Kelvin wave variability near the eastern boundary as far as 80°E. Although long equatorial waves are primarily forced by the changes in the winds during the monsoon transitions, reflections have a strong influence on the ocean's variability over a large part of the basin on both seasonal and interannual time scales. The constructive/destructive interaction

between the wind forcing and the wave reflection is responsible for the Kelvin/Rossby wave seasonal cycle to show a semi-annual (annual) period near the western (eastern) boundary. Senan et al. (2003) have reported strong WWBs associated with summer monsoon intraseasonal oscillations that can drive monsoon jets in the eastern EIO. They have also reported distinct equatorial WWBs associated with the MJO in January–March which do not produce equatorial jets in the ocean.

Masson et al. (2004) have examined the role of near-surface stratification on the fall WJ in an OGCM. The inclusion of salinity favors a stronger WJ that extends further eastward. A sporadic barrier layer increases the jet speed by trapping wind momentum into a thinner mixed layer. In an OGCM simulation, Han et al. (2004) have found that intraseasonal atmospheric forcing acts to weaken the equatorial seasonal surface currents. Amplitudes of the boreal spring and boreal fall WJs, and the westward surface current during January–March are reduced by as much as 15–25 cm/s by atmospheric intraseasonal forcing and the strengths of the rectification exhibit significant interannual variability. In a reduced gravity model simulation, Rahul Chand Reddy et al. (2004) have found the westward propagation of twin anticyclonic gyres on either side of the equator soon after the termination of the boreal spring and boreal fall WJs. They form at the front of a Rossby wave packet generated by the reflection of the WJs from the eastern boundary of the basin. They are likely either Rossby solitons or result from the nonlinear interactions between the WJs and the Rossby wave front. Han (2005) has shown dominant spectral peaks at 30–60 and 90 days in the sea level observations of the EIO. The 90 day sea level oscillation in the EIO was also shown by Schouten et al. (2002). The quick look analysis of the ADCP data at the same location of this study (November 2000–October 2001) by Masumoto et al. (2005), has shown dominant periods of variability in the upper layer ZCs in the intraseasonal frequency band with period of 30–50 days with strong correlation with the local wind variability. In addition, a zone of strong vertical shear of the ZC and a distinct EUC with semiannual period are also observed. Using an OGCM, Yuan and Han (2006) have studied the roles of the equatorial waves and the western boundary reflection on the seasonal circulation of the EIO. They have shown that the alongshore winds off the east coast of Africa and the Rossby waves in the off-equatorial areas contribute significantly to the annual harmonics of the equatorial Kelvin waves at the western boundary. The semiannual harmonics of the Kelvin waves, on the other hand, originate primarily from a linear reflection of the equatorial Rossby waves. Because of the reflections, the second baroclinic mode resonates with the semiannual wind forcing; that is, the semiannual ZCs carried by the reflected waves enhance the wind forced currents at the central basin. The Rossby waves are found to have a larger contribution to the observed equatorial semiannual oscillations of surface ZCs than the Kelvin waves. The westward progressive reversal of seasonal surface ZCs along the equator in the observations is primarily due to the Rossby wave propagation. Based on analysis of both data and model simulations for the period 1991–2000, Han et al. (2006) have found that atmospheric intraseasonal oscillations play a significant role in causing irregularity of the two IOD events during 1994 and 1997 and the premature termination of the weak IOD event during 1991. Of particular interest is a basin-wide, wind driven oceanic resonance with a period near 90 days, involving the propagation of equatorial Kelvin and first meridional mode Rossby waves across the basin. Before the onset of the strong 1997 IOD event, wind variability had significant power near 90 days and the resonance was strongly excited. From the deployment of current meter moorings on the equator in the EIO, Murty et al. (2006) have shown strong semiannual variability in the ZC with superimposed intraseasonal oscillations with periods 30–50 days and the amplitude of the semiannual signal progressively decreases with depth.

Sengupta et al. (2007) have reported that along the equator, moderate westerly winds are punctuated by strong 10–40 day bursts which force swift intraseasonal (20–50 day) eastward equatorial jets in boreal spring, boreal summer and boreal fall. The zonal momentum balance is between the local acceleration, surface wind stress, and ZPG, while non-linearity deepens and strengthens the eastward current. The westward ZPG force associated with the thermocline deepening towards the east rapidly arrests eastward jets and, subsequently generates weak westward flow. In agreement with the direct observations in the eastern EIO, they have shown in an OGCM simulation that the boreal spring jet is a single intraseasonal event, there are intraseasonal jets in summer, and the boreal fall jet is long lived but strongly modulated on intraseasonal time scale. The ZPG force is almost always westward in the upper 120 m, and changes sign twice a year in the 120–200 m layer. Transient EUCs in early boreal spring and late boreal summer are associated with semiannual Rossby waves generated at the eastern boundary following thermocline deepening by the boreal spring and boreal fall jets. An easterly wind stress is not necessary to generate the undercurrents.

Fu (2007) examined all the available time series of sea surface height anomalies (SSHA), surface winds and SST over the EIO to characterize the observed intraseasonal variability. The frequency spectrum of the wind stress revealed peaks at the seasonal cycle and its higher harmonics at 180, 120, 90 and 75 days. The semiannual SSHA variability is characterized by a basin mode involving Rossby and Kelvin waves, leading to a nodal point (amphidrome) of phase propagation on the equator at the center of the basin. For

the semiannual period and the size of the basin, the resonance involves the second baroclinic vertical mode of the ocean. Modes at 90 and 60 days are only found in the eastern part of the basin, where the wind forcing at these periods is primarily located. During the peak of the 2006 IOD from September to November, the current data at the same location of this study revealed anomalous subsurface structures (Horii et al. 2008). The surface current anomaly at 10 m depth observed by the TRITON buoy was westward consistent with the direction of the anomalous easterly wind prevailing over the buoy location. In the layer between 50 and 150 m depths eastward current anomalies were observed during September to November 2006. Masumoto et al. (2008) have reported eastward subsurface zonal flow under westward flowing surface current during October–November around 80.5°E on the equator during the same IOD year. The influence of IOD on the intraseasonal ZCs in the eastern EIO is examined by Iskandar et al. (2008). They have shown that during negative IOD events the intraseasonal ZCs are mostly dominated by the first two modes. On the other hand, contributions from the higher modes to the intraseasonal ZCs significantly increase during positive IOD events. This is attributed to the change in the background stratification associated with the IOD events; sharp pycnocline in the eastern basin during positive IOD events causes the wind forcing to project more on to higher modes.

Hase et al. (2008) have examined the time series of temperature and salinity measurements collected by the TRITON buoys moored in the eastern EIO. Their spectral analysis indicates that the dominant temperature signals in the surface layer and below the thermocline have intraseasonal and semiannual timescales respectively. The semiannual isotherm deepening in the thermocline appears clearly during the monsoon transitions, and indicates vertical phase shift below the thermocline corresponding to a value between the characteristic speeds of the second and third baroclinic modes. The correlation between the surface ZW stress on the equator and the depth of 20 °C isotherm (D20) variation shows that the forcing region of the semiannual isotherm variation is located around 68°E–78°E on the equator. The estimation of characteristic speed from the lag between these variations also shows a value between the second and third vertical-mode gravity waves. Iskandar and McPhaden (2011) have shown that the near-surface layer responds directly to intraseasonal zonal wind stress forcing and that subsequently energy radiates downward and eastward in the thermocline in the form of wind-forced equatorial Kelvin waves. At periods of 30–70 days, zonal velocity tends to be stationary in the directly forced region along the equator owing to the competing contributions of Kelvin and Rossby waves. In contrast, at 70–110 day periods, zonal velocity propagates westward despite eastward propagation of zonal wind stress because of the combined influence of eastern boundary generated and wind-forced Rossby waves (Nagura and McPhaden 2012).

Thus most of the earlier observational studies are based on relatively short records while the data set utilized in the present study is long enough and reliable to represent as a benchmark data set for model validation on several time scales. In the present study, all the available full 8 year (2001–2008) record of ADCP data is utilized to provide a comprehensive description and to explain the observed zonal flow at the Equator, 90°E on seasonal, intraseasonal and interannual time scales with major focus on the following issues.

- The role of equatorial winds and alongshore winds off the Somaila coast on the observed ZC field
- The role of propagating waves in the equatorial waveguide on the observed ZC field
- The role of ZPG along the equator on the observed ZC field
- The influence of salinity induced near-surface stratification on the observed ZC field
- The potential influence of ZCs and equatorial waves on the evolution of SST along the equator.

3 Observations and methodology

Several types of archived historic in situ measurements and the relevant satellite data are assembled and utilized in this study to describe and explain the observed variability of the ZCs at 90°E on the equator in the Indian Ocean. An upward looking ADCP was deployed by JAMSTEC around 400 m depth at the Equator, 90°E in the core of the warm pool region of the eastern EIO (Fig. 1) on 14 Nov, 2000 and the hourly data are being recorded since then uninterruptedly at 8 m vertical resolution. The data above 40 m depth are not accurate due to surface reflections and hence not considered in this study. These measurements are longer in duration than the earlier measurements made near Gan Island (Knox 1976; McPhaden 1982), in the western EIO (Luyten and Roemmich 1982) and south of Sri Lanka (Schott et al. 1994; Reppin et al. 1999). The details of ADCP mooring are given by Masumoto et al. (2005) and Iskandar et al. (2009). This data set represents the longest record for more than 8 years and can reveal rich variability in the interior and can be used for model validation. The total data set collected from November, 2000 to March, 2009 is utilized in this study to characterize the observed flow patterns between 40 and 350 m depths. The current data collected from PMEL ADCP mooring deployed at the Equator, 80.5°E during October, 2004–August, 2008 are also utilized to compute the zonal propagation of Kelvin waves in the equatorial wave guide (Fig. 1). A TRITON buoy with CTD sensors (Kuroda 2002) was deployed by JAMSTEC at 1.5°S and

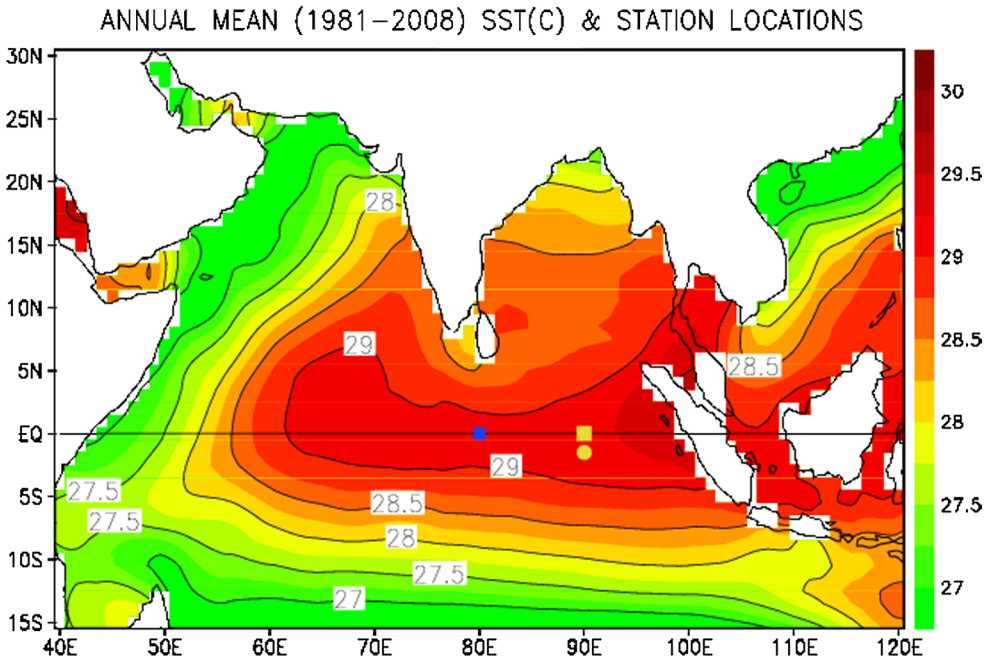

Fig. 1 Station locations—JAMSTEC ADCP mooring at the Equator, 90°E (*yellow square* on the equator), JAMSTEC TRITON Buoy at 1.5°S, 90°E (*yellow circle* south of yellow square) and PMEL ADCP mooring at the Equator, 80.5°E (*blue square* on the equator) and the warm pool region (SST > 28 °C) in the TIO

90°E on 26 October, 2001 to record the vertical profiles of temperature and salinity in the topmost 750 m water column (Fig. 1). As the vertical resolution of the sensors of the TRITON mooring is not fine, the spline method of Akima (1970) is utilized to interpolate data in the vertical and in time when data were missing on very few occasions. These data are utilized to characterize the observed barrier layer thickness (BLT) and stratification in the pycnocline. The multi-year QuikSCAT surface winds (Wentz et al. 2001) are utilized to assess their impact on the observed zonal flow and the propagating waves in the EIO. The AVISO merged and blended multi-year sea surface height anomaly (SSHA) data are utilized to characterize the signature of the propagating Kelvin and Rossby waves. The multi-year TRMM TMI SST (Wentz et al. 2000) are utilized to characterize the background SST in the EIO during the years 2001–2008. The objectively analyzed surface net heat flux generated by Yuet al. (2008) are utilized to explain the contrasting SST distributions observed along the equator during 2001 and 2003. The depth of 20 °C isotherm (D20) data extracted from the Coriolis vertical thermal structure, NOAA outgoing long wave radiation (OLR) data (Liebmann and Smith 1996), and the OSCAR currents (Lagerloef et al. 1999; Johnson et al. 2007) for all the available years are also utilized to characterize the basin scale variability in the spectral domain for the TIO. The bandpass filtering of BLT data is done following Duchon (1979). A large sample of 2048 points is considered for the estimation of power spectra and cross spectra of the ZWs and the ZCs following Hino (1977). The sources, periods, accuracies and resolutions of the data sets utilized in this study are listed in Table 1.

4 Analysis

4.1 Spatio-temporal variability of OLR, ZW, SSHA, D20 and ZC in the TIO

To set the background for this study, all the available historic data sets are assembled and synthesized to construct a comprehensive framework to portray the observed spatio-temporal variability of surface ZC and the related parameters such as OLR, ZW, SSHA and D20 through their basin-scale variance preserving power spectral density distributions following Hino (1977). The amplitudes for most prominent temporal modes such as annual, semiannual, 90, 60–90, 30–60, and 10–30 are shown in Fig. 2 for the entire TIO. The spectral distribution of OLR shows strong annual mode in the Indian summer monsoon domain extending from the eastern Arabian Sea to east of Myanmar. However, no signal is seen in the equatorial region with the lone exception of the maritime Indonesian islands in the far-east. The semiannual signal is prominent over the Indian summer monsoon trough zone and in the southern Arabian Sea. On the intraseasonal time scales (10–90 days) the signals encompass the entire warm pool region with their cores lying in the eastern EIO and the western Bay of Bengal. The spectral distribution of ZW shows strong annual mode over the entire north Indian Ocean and over the region approximately between the south of the equator and 15°S. In tune with the OLR, on the annual mode the ZW signal is also relatively weaker over the equatorial region. The semiannual signal is stronger over the western equatorial region a little away from the African coast, over

Table 1 Data sources, periods, accuracies and resolutions

Parameter	Source	Period	Accuracy	Spatio/temporal resolution
ADCP ZC	JAMSTEC, Japan	Nov, 2000–Mar, 2009	1 % 5 mm/s	40–350 m, @10 m, 1 day
TRITON CTD Temperature Salinity	www.jamstec.go.jp/TRITON/real_time/php/top.php	Oct, 2001–Sep, 2007	0.002 °C 0.04PSU	1.5, 25, 50, 75, 100, 125, 150, 200, 250, 300, 500, 750 m in the vertical and 1 day
PMEL ADCP ZC	PMEL, USA	Oct, 2004–Aug, 2008	1 % 5 mm/s	25–330 m @5 m, 1 day
QuikSCAT ZW	www.ssmi.com	2001–2008	2 m/s	0.25°, 1 day
AVISO Blended SSHA	www.aviso.oceanobs.com	2001–2008	2.5–4 cm	0.33°, 7 days
TRMM TMI SST	www.ssmi.com	2001–2008	~0.5 °C	0.25°, 1 day
WHOI Surface Net Heat Flux	oaflux.whoi.edu	2001 and 2003	~25 W/m^2	1.0°, 1 day
NOAA OLR	www.cdc.noaa.gov/cdc/data.interp_OLR.html	1981–2008	10 W/m^2	2.5°, 1 day
Coriolis D20	eftp.ifremer.fr	2001–2007	~10 m	1.0°, 10 days
OSCAR ZC	www.dapper.pmel.noaa.gov/dapper/oscar/world-unfilter.nc	1992–2008	–	1.0°, 5 days

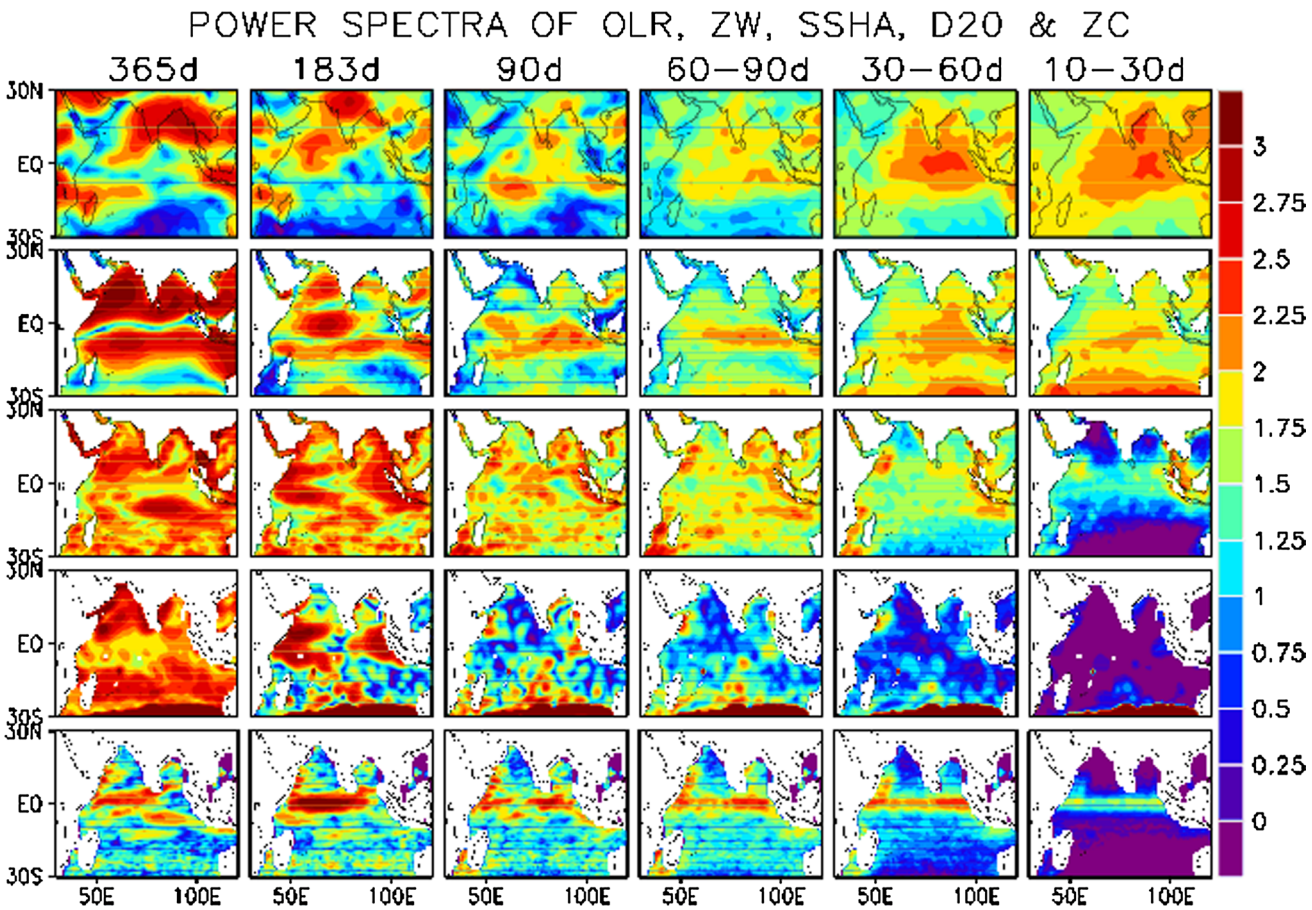

Fig. 2 Amplitudes of variance preserving power spectra of NOAA OLR (*topmost panel*), QuikSCAT ZW (*2nd topmost panel*), AVISO SSHA (*3rd topmost panel*), Coriolis D20 (*4th topmost panel*) and OSCAR ZC (*bottommost panel*) for the temporal modes such as annual, semiannual, 90, 60–90, 30–60, and 10–30 day for the TIO. (Units are arbitrary and are multiplied by appropriate scale factors for easy comparison.)

the central Arabian Sea, the Bay of Bengal and along a narrow east–west band south of the equator. With the increase in frequency of the mode, the signal shifts from the western EIO to the central and eastern EIO where the core of the warm pool is located. The spectral distributions of both SSHA and D20 show strong annual mode in the southern Arabian Sea and in the region south of the equator where the signature of the westward propagating Rossby waves is most pronounced (McCreary et al. 1993; Masumoto and Meyers 1998; Basu et al. 2000; Brandt et al. 2002). The signals at the semiannual mode for both SSHA and D20 are most pronounced in the north and south of the equator in the western EIO caused by westward propagating Rossby waves and their western boundary reflections (Le Blanc and Boulanger 2001; Fu 2007). The eastern EIO also shows strong signals both in the SSHA and D20 primarily caused by the eastward propagating and coastally trapped Kelvin waves and the westward excited Rossby waves. At 90 and 60–90 day modes, the signals in both the fields are stronger off the Sumatra coast primarily due to coastal Kelvin wave activity (Iskandar et al. 2005). The spectral distribution of ZC shows strong signals confining to the equator and near-equatorial region at all the temporal modes. In close agreement with the distributions shown in all the atlases on the near-surface circulation derived from ship drift vectors (KNMI 1952; Cutler and Swallow 1984; Rao et al. 1991; Mariano et al. 1995) and from satellite measurements (Rao et al. 2009b) the annual mode shows large signals in the regions of the Summer and Winter Monsoon Currents north of the equator and of the South Equatorial Current south of the equator while the semiannual mode shows a very pronounced signal only in the western EIO a little away from the east African coast caused by Wyrtki jets where a corresponding signal is also seen in the ZW field. Pronounced signals are also seen at the intraseasonal mode off the Somalia coast and in the eastern EIO as reported by Sengupta et al. (2001a).

4.2 Evolution of seasonal cycle of ZWs along the equator in the Indian Ocean

The observed climatology of the annual cycle (1999–2008) of the QuikSCAT (Wentz et al. 2001) surface ZWs along the equator shows a distinct semiannual mode with

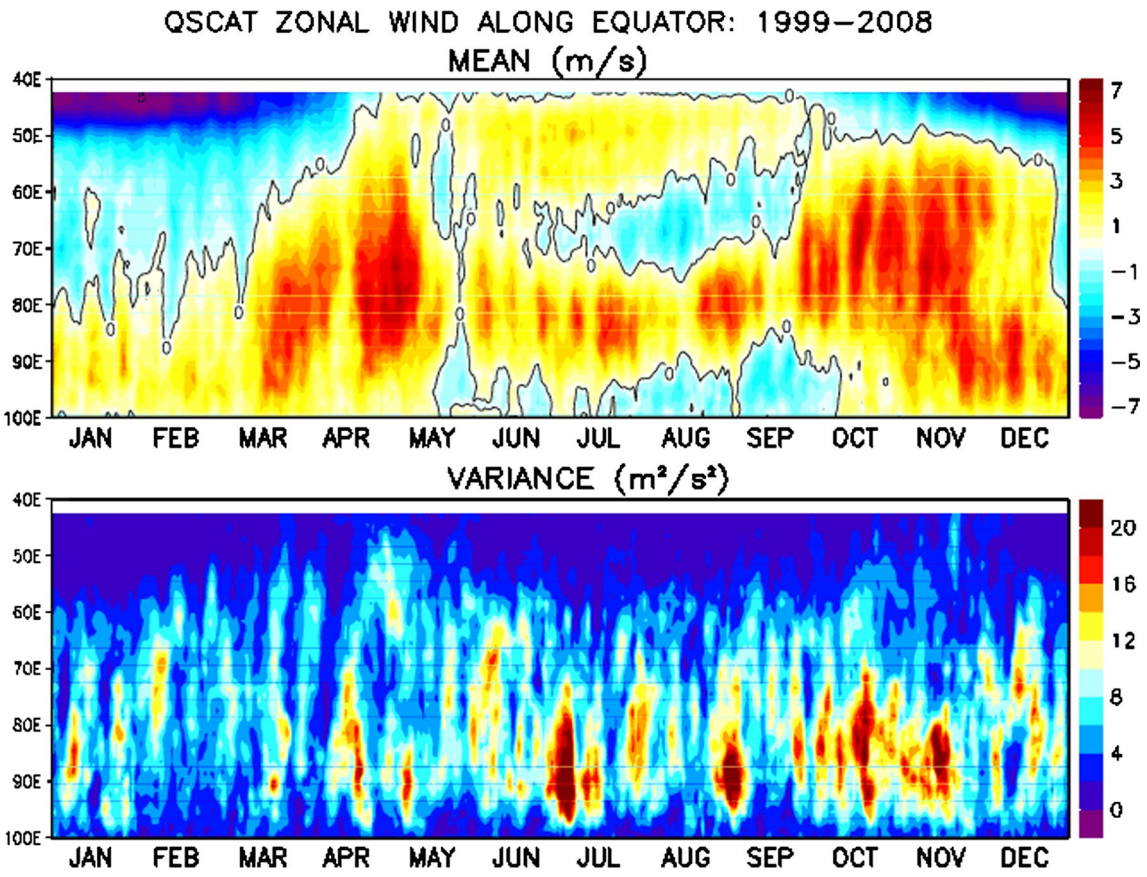

Fig. 3 Observed annual cycle of mean (m/s) and variance (m^2/s^2) of QuikSCAT surface ZWs along the equator (40°E–100°E) for the period 1999–2008

embedded intraseasonal oscillations on time scales of 10–40 day periods peaking during the transitions between both the monsoons (Knox 1976; McPhaden 1982; Rao et al. 2009a; Fig. 3). The patch of westerly winds is stronger and wider in spatio-temporal extent during the boreal fall transition than during the boreal spring transition. The amplitude of intraseasonal ZW fluctuations in the central and the eastern EIO is as large as the semiannual component as suggested by Goswami and Sengupta (2003). Between 60°E and 100°E, the westerly (easterly) winds blow over relatively longer (shorter) duration and are relatively stronger (weaker). During December–March along the western equator the easterly winds are relatively stronger. The variance of the westerly ZWs is larger over the eastern EIO almost throughout the year showing modulations in the intensity. Strong patches of variance are seen in the eastern EIO during the summer monsoon and the boreal fall transition and to a lesser degree during the boreal spring transition primarily driven by the variability of the organized moist convection in the atmosphere (Reverdin et al. 1986).

The WWBs occur on intraseasonal time scale almost throughout the year with speeds in excess of 5 m/s shown in Fig. 4 are the most striking features of the seasonal cycle of the ZW field over the central and eastern EIO. They show a longer temporal manifestation during the boreal fall transition than during the boreal spring transition. Analysis of historic ship reports (1954–1976) by Reverdin et al. (1986) has shown strong wind anomalies forced by the rainfall anomalies in the central and eastern EIO during the boreal fall transition. The zonal scale of WWBs is comparable to the size of the basin only during both the transition periods. A distinct year-to-year variability in the distribution of WWBs is seen during the observational record of 2001–2008. During some years, these WWBs also occur during the summer monsoon season but mostly confining to the eastern EIO. The WWBs are more pronounced during the summer monsoon seasons of certain years such as 2001, 2002, 2004 and 2005. During the boreal winter, easterlies occur in the western EIO and they extend occasionally eastward. These easterlies are also seen in the central and eastern EIO during summer monsoon season, more

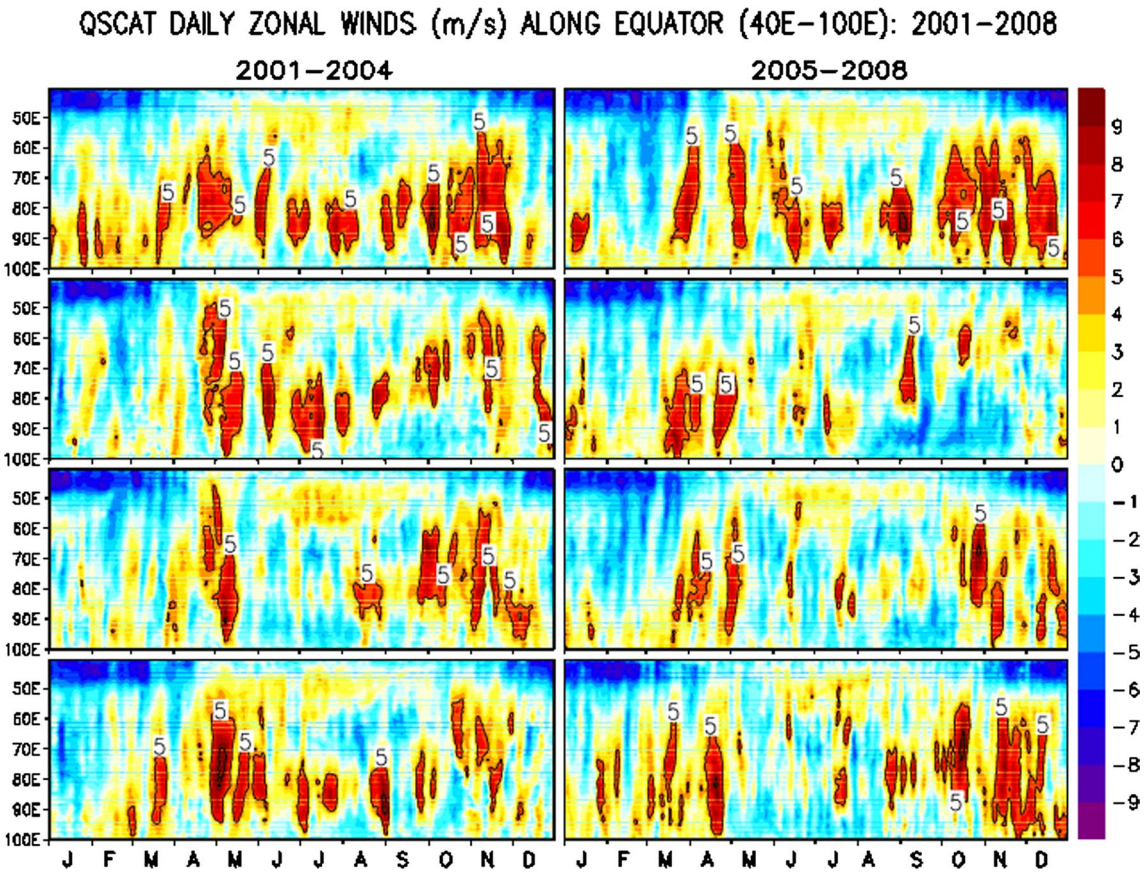

Fig. 4 Evolution of 3 day moving averages of QuikSCAT surface ZWs (m/s) along the equator (40°E–100°E) in the Indian Ocean during the years 2001–2008 (years increasing *downward in the vertical panels*)

pronounced during the years such as 2003, 2006, 2007 and 2008 when the WWBs are absent. The occurrence of easterlies also clearly shows up the signature of the IOD event over the eastern EIO during August–November, 2006.

4.3 Evolution of seasonal cycle of ZCs at the Equator, 90°E

The daily evolution of ZCs at the Equator, 90°E between 40 and 350 m depths during the individual years 2001–2008 (Fig. 5) shows that the observed flow patterns are unique during each year. As reported by the earlier investigators, the near-surface layer is characterized by strong eastward flowing intraseasonal jets that are more pronounced during both the monsoon transitions. These eastward jets are accelerated by the ZW stress, but decelerated by the time-varying ZPG resulting in subsequent westward flow lasting a month or longer (Knox 1976). These jets are almost absent during January–March as also reported by Sengupta et al. (2007) in their model simulation. McPhaden (1982) has suggested that these jets are the manifestation of a forced 30–60 day ocean response based on observations near the Gan Island. In general, more intraseasonal events in the ZC are seen during the boreal fall transition in comparison to that of the boreal spring transition. Relatively short lived intraseasonal jets are also seen during the summer monsoon season, but with large internannual variability. For example, these intraseasonal jets are most (least) pronounced during 2005 (2007). The subsurface eastward flow in the upper thermocline (80–160 m) named as the equatorial undercurrent (EUC) is a transient feature related to propagating wave dynamics (Schott and McCreary 2001). The eastward flowing EUC shows strong seasonal asymmetry—the EUC is more pronounced during March–April than that of during October–November, with the only exception of the IOD year 2006. Large interannual variability during both the monsoon transitions is primarily attributed to differences in the surface ZW field as reported earlier by Knox (1976) and Iskandar et al. (2009). The boreal fall transition EUC was almost absent during 2001, 2003, 2007 and 2008 while it was more pronounced during 2002, 2004 and 2006 which is an IOD year. Similarly, the EUC during the boreal spring transition also shows large interannual variability. It is most (least) pronounced during 2003,

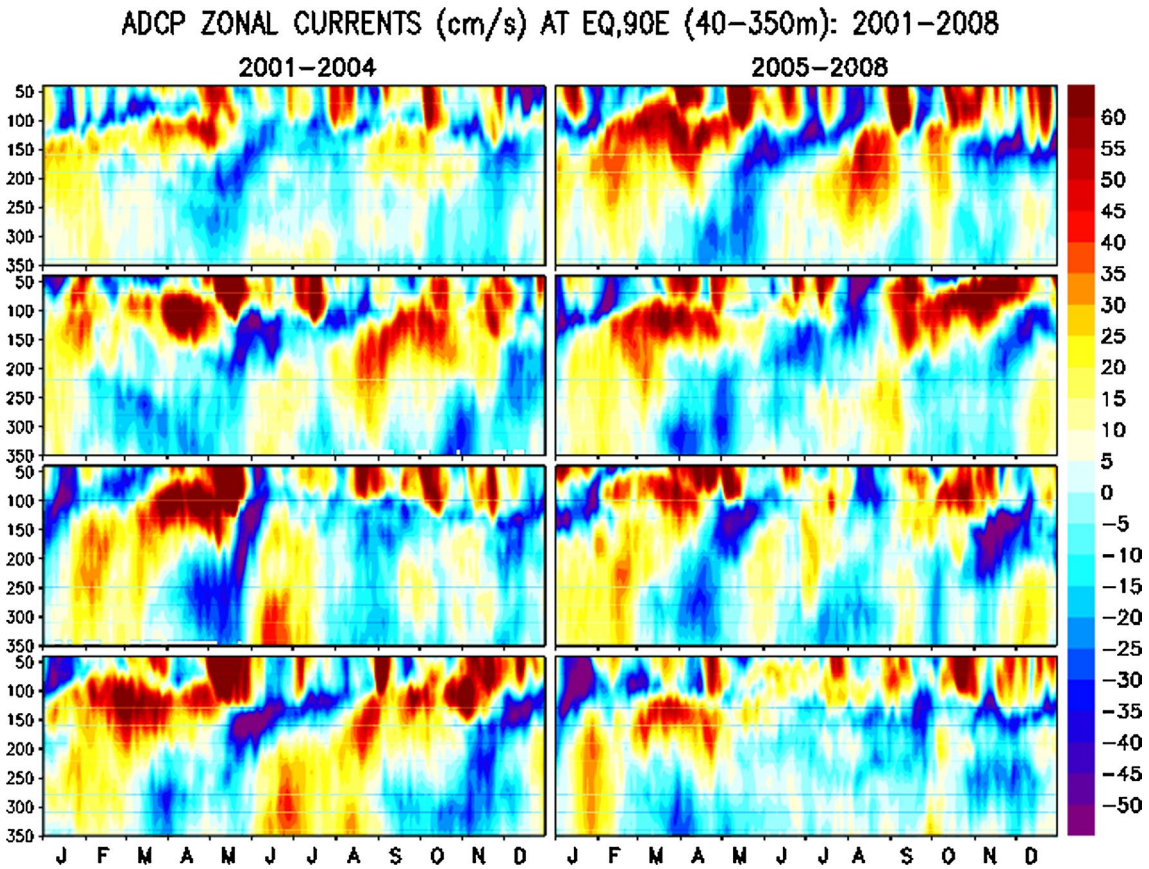

Fig. 5 Evolution of 3 day moving averages of JAMSTEC ADCP ZCs (cm/s) at the Equator, 90°E in the 40–350 m water column during 2001–2008 (years increasing *downward in the vertical panels*)

2004, 2005 and 2006 (2001 and 2008). Another interesting feature is the observed interannual variability of the westward flowing undercurrent in the subsurface layer. During normal years, the westward flow occurs twice a year with upward phase propagation. But during years when the WWBs are replaced by easterlies over the central and eastern EIO during the summer monsoon season as seen in Fig. 4, an anomalous westward flow occurs during the height of the summer monsoon season as seen during years such as 2003 and 2007. Further, a careful examination also reveals that, the annual cycle of the ZC is generally weaker during 2001 and 2008 in comparison with the rest of the years. The probable reasons for these differences on interannual time scale will be examined in the subsequent sections. In addition, the signature of the IOD event that occurred during 2006–2007 is also clearly seen in the observations in accordance with Gnanaseelan et al. (2012).

The observed multi-year (2000–2009) averaged daily ADCP ZC between 40 and 350 m depths recorded at the Equator, 90°E (Fig. 6) shows periodic east–west reversals throughout the water column predominantly at the semiannual frequency. The associated upward phase propagation indicates the influence of eastward propagating Kelvin waves. Data from current meter moorings in the western EIO have also shown upward phase propagation in the semiannual signal in the thermocline (McPhaden 1982; Luyten and Roemmich 1982; Reppin 1999). In general, the ZC is stronger in the near-surface layer in comparison to that of in the subsurface layer. The semiannual signal is more pronounced in the subsurface layer while it gets masked by the occurrence of intraseasonal jets in the near-surface layer (Webster et al. 2002; Senan et al. 2003; Masumoto et al. 2005; Sengupta et al. 2007). In the near-surface layer, the ZC mostly flows eastward with sporadic intensifications occurring on intraseasonal time scale during March–July and September–December. It reverses its flow towards west only during January–February and August. The EUC is most pronounced in the depth range of 80–160 m during March–April and October–November. In the upper thermocline (100–200 m) a westward flowing undercurrent with upward phase propagation is also seen during November–February. Another westward flow first appears at depths of 250–350 m in March–April with upward phase propagation and generally peaks near the surface by August. The

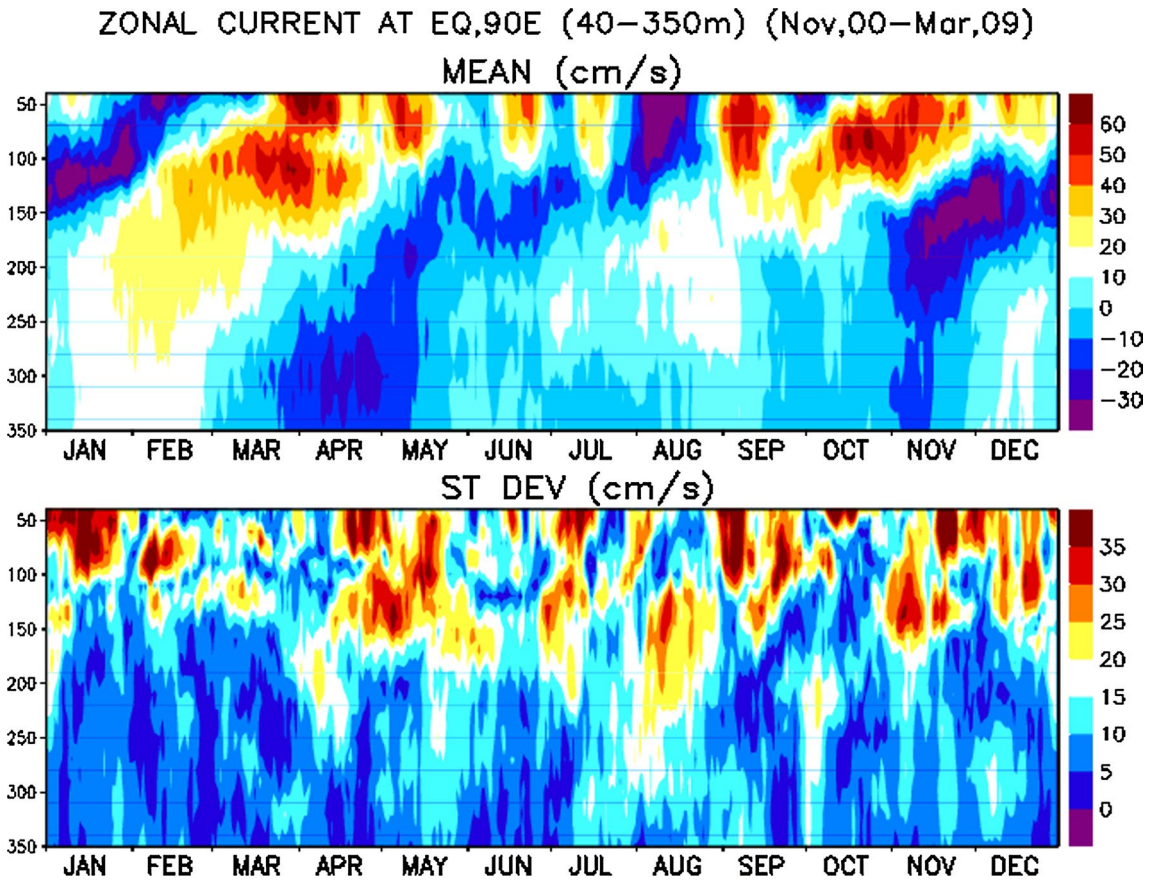

Fig. 6 Annual cycle of JAMSTEC ADCP daily mean (cm/s) and standard deviation (cm/s) of ZC at the Equator, 90°E in the 40–350 m water column during the period 14 November, 2000–21 March, 2009

direction and the intensity of the flow in the near-surface layer are determined by the prevailing ZWs through local frictional coupling (Yoshida 1959; O'Brien and Hurlburt 1974; Knox 1976; Philander and Pacanowski 1980; Cane 1980; McPhaden 1982; Philander 1990; Han 2005; Masumoto et al. 2005; Sengupta et al. 2007). The equatorial ocean responds to westerly winds by developing accelerating eastward jets in a few days, and intraseasonal WWBs are capable of producing strong equatorial jets. On the other hand the direction and the intensity of the flow in the subsurface layer are determined by the ZPG set up by both the surface ZW field and the propagating Kelvin and Rossby wave fields in the equatorial wave guide (Bubnov 1994; Senan et al. 2003; Sengupta et al. 2007; Nagura and McPhaden 2008; Iskandar et al. 2009). The variance of ZC is much stronger in the near-surface layer and appears patchy primarily caused by variability both on intraseasonal and interannual time scales. It is much weaker during February–March when the intraseasonal jets in ZC field are also absent in the near-surface layer.

4.4 Evolution of seasonal cycle of SSHA along the equator in the Indian Ocean

Both the boreal spring and the boreal fall WJs lead to increase the east–west slope of the thermocline and the mean sea level in the EIO (Wyrtki 1973; Bubnov 1994). When westerly (easterly) winds blow over the equator, downwelling (upwelling)-favorable equatorially trapped Kelvin waves radiate into the eastern ocean, deepening (shoaling) the thermocline there. These waves reflect from the eastern boundary as packets of coastally trapped Kelvin and Rossby waves, spreading the deepening/shoaling well off the equator. Rossby waves can also be generated in the off-equatorial regions through forcing by a patch of anticyclonic (downwelling) Ekman pumping in

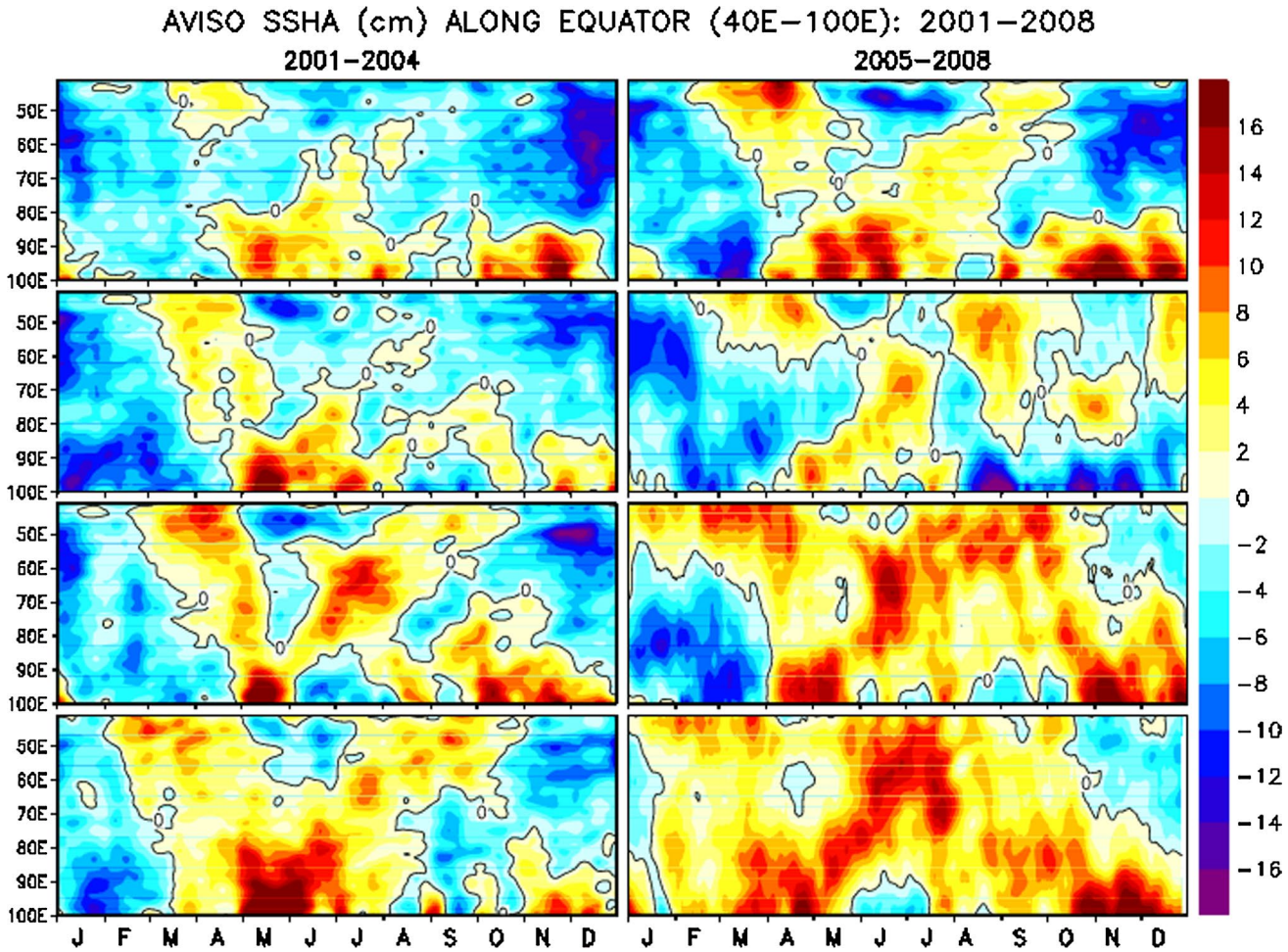

Fig. 7 Evolution of 3 day moving averages of AVISO SSHA (cm) along the equator (2°S–2°N) during 2001–2008 (years increasing *downward in the vertical panels*) (only *zero line* is contoured to highlight the eastward propagating signatures of the downwelling Kelvin waves during boreal spring and boreal fall seasons)

the eastern ocean. Then downwelling favorable Rossby waves radiate from the forcing region, deepening the thermocline in the western ocean (Schott et al. 2009). In the Indian Ocean, the energy imparted by the surface wind field is carried eastward along the equatorial wave guide as both downwelling and upwelling Kelvin waves and traverse around the rim of the Bay of Bengal and off the west coast of Indonesia. The signature of this wave propagation along the equator is clearly seen from the satellite derived altimetry and surface wind measurements (Iskandar et al. 2009; Rao et al. 2010). The WWBs produce downwelling Kelvin waves that propagate eastward along the equator (O'Brien and Hurlburt 1974; McPhaden 1982; Visbeck and Schott 1992; Jensen 1993; McCreary et al. 1993; Han et al. 1999, 2001). When these WWBs weaken during July–August or are replaced by easterlies during boreal winter, the upwelling Kelvin waves are triggered and propagate eastward along the equator. In a year, two pairs of upwelling and downwelling Kelvin waves propagate eastward alternately (Iskandar et al. 2009; Rao et al. 2010). The signatures of these upwelling and downwelling Kelvin waves are best captured in the longitude-time fields of SSHA in the EIO (Fig. 7). These fields show strong eastward propagating semiannual signals along the equator. The deepening (shoaling) of thermocline and the associated increase (decrease) of SSHA during April–June (January–March) and October–December (August–September) is a clear manifestation of the downwelling (upwelling) Kelvin waves. In addition, these Kelvin waves also reflect (trigger) Rossby waves that propagate westward both along and off the equator (Potemra et al. 1991; Yu et al. 1991). These waves in turn contribute to the observed semiannual variability seen in the ZC field along the equator. Although the SSHA field is relatively weaker corresponding to weaker ZC field during 2001, such correspondence is not seen during 2008 for reasons unclear. It is interesting to note that the Indonesian Through flow along Makassar Strait has also shown anomalous shoaling of the core of the maximum flow with warmer waters during 2007 and 2008 in association with three consecutive

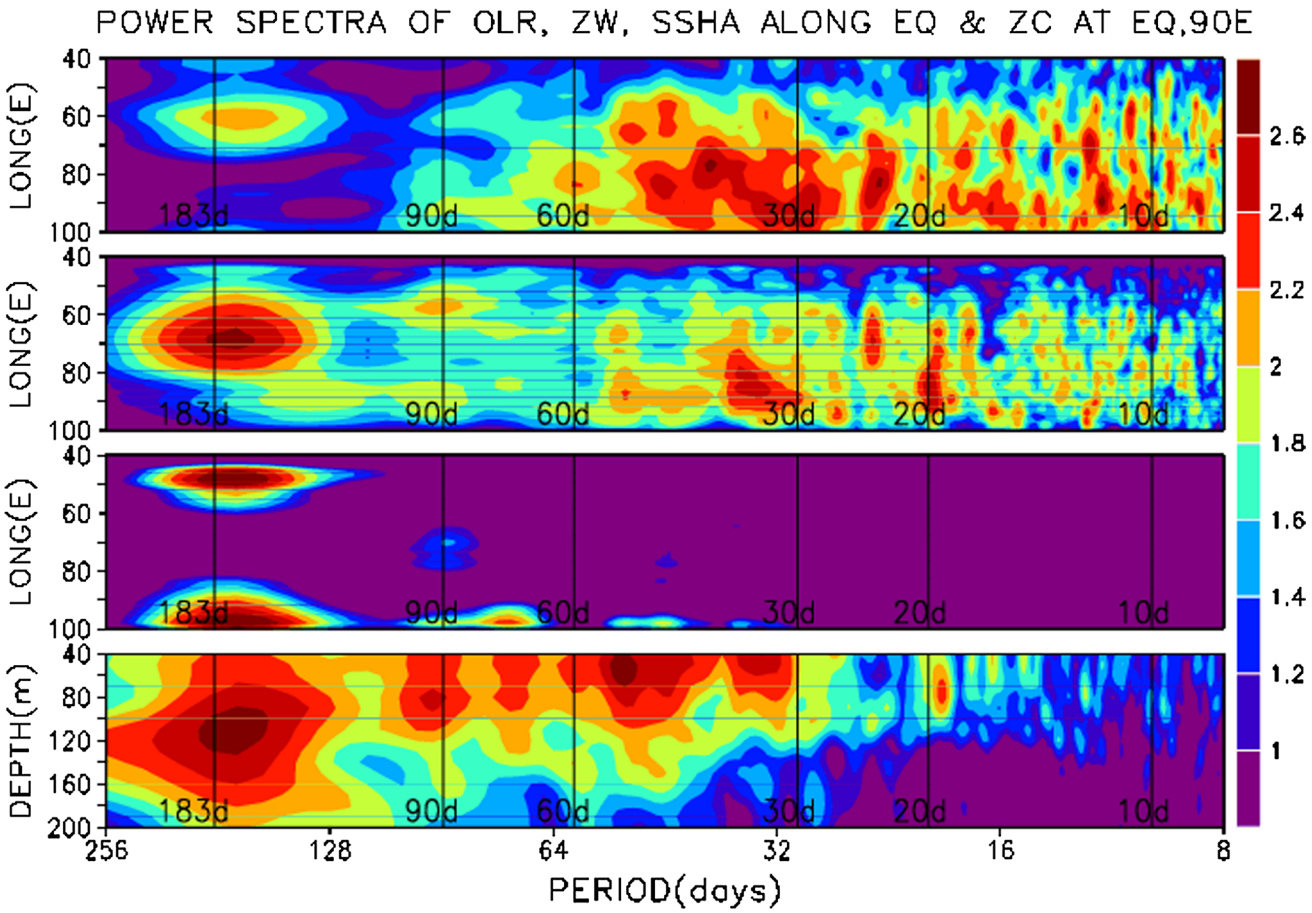

Fig. 8 Amplitudes of variance preserving power spectra of OLR (*topmost panel*), ZW (*second topmost panel*), and SSHA (*third topmost panel*) along the equator and ZC (*bottom panel*) at the Equator, 90°E. (Units are arbitrary and are multiplied by appropriate scale factors for easy comparison. *Vertical lines* indicate the most prominent periods for easy reference.)

positive IOD events during 2006–2008 (Gordon et al. 2009).

4.5 Spectra of OLR, ZW, SSHA along the equator and ZC at the equator, 90°E

The observed variability of the ZC at the Equator, 90°E and related parameters such as OLR, ZW, SSHA along the equator is synthesized through their variance preserving power spectral distributions following Hino (1977; Fig. 8). The amplitudes of power spectra are shown for periods in the temporal range of 8–256 days as the annual frequency is relatively weaker along the equator. In the western EIO, the OLR spectra show a strong signal at the semiannual period associated with seasonally reversing monsoons. On the other hand, in the eastern EIO, pronounced intraseasonal signals associated with atmospheric moist convection with time periods 10–60 days are the most notable ones. The spectra of the surface ZW show most pronounced signal in the central EIO at the semiannual period in agreement with Fu (2007). In tune with OLR, it also shows pronounced intraseasonal signals with time periods 10–60 days covering the MJO band in the central and eastern EIO. In addition, a relatively weaker signal at 90 day period is also seen in the western EIO. Interestingly the spectra of SSHA show two major peaks, one with its core lying around 50°E and the other with its core lying around 95°E, both slightly away from the coastal boundaries consistent with earlier studies (Le Blanc and Boulanger 2001; Fu 2007). Another minor peak around 75 days is also seen very close to the eastern rim of the EIO. At the semiannual frequency, the ZC shows a spectral peak in the upper thermocline (core in the depth range of 80–160 m where the EUC is located) while the other peaks are noticed in the near-surface layer at intraseasonal periods of 30–90 days. It is quite clear that the coupling between the surface ZW field from 60°E to 80°E along the equator and ZC in the upper thermocline at the Equator, 90°E at the semiannual frequency is quite strong in agreement with Hase et al. (2008). Earlier modeling studies (Yuan and Han 2006; Sengupta et al. 2007) have clearly shown that the peak in the upper thermocline is in response to the ZPG set up by the ZW and propagating wave fields. The intraseasonal winds cause the 30–90 day peaks within the near-surface layer. A good one to one correspondence is seen between the peaks of ZC and ZW at 30–40 day period. However, it is interesting to note that 40–60 day peak is relatively stronger in ZC although a corresponding stronger peak is not seen in the ZW. The peak at 90 days in the ZC is also pronounced although the corresponding ZW peaks both in the west and east are not strong. In an OGCM simulation, Han (2005) has found near the surface, the spectral peaks of currents

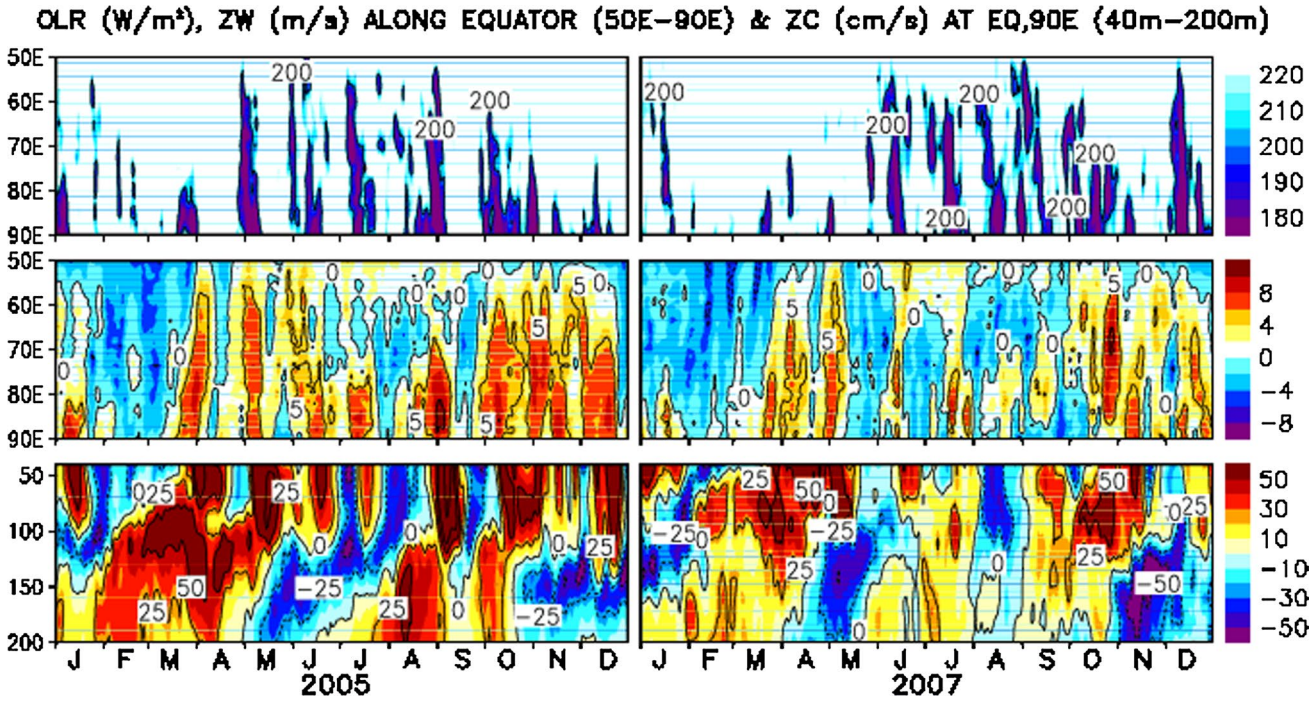

Fig. 9 Evolution of 3 day moving averages of NOAA OLR (W/m^2) (2.5°S–2.5°N) (*top panel*), QuikSCAT ZW (m/s) (1°S–1°N) along the equator (*middle panel*) and JAMSTEC ADCP ZC (cm/s) at the Equator, 90°E (*bottom panel*) during two contrasting years 2005 and 2007. (OLR >230 W/m^2 is suppressed to highlight organized moist atmospheric convection. Positive values of ZW speed @ 5 m/s are only contoured to highlight WWBs)

and sea level at the 30–60 day period are directly forced by winds that peak at 30–60 days. At the 90 day period, both the observed and the model simulated sea level anomaly fields show that equatorial Kelvin and first meridional mode Rossby wave structures are forced by the 90 day winds. Han (2005) has also shown that this selective response arises mainly from the resonant excitation of the second baroclinic mode waves by the 90 day winds. In this case, the Rossby waves reflected from the eastern boundary enhance the directly forced response in the ocean interior, strengthening the 90 day peak. The 90 day time scale is intrinsic to the equatorial adjustment of the Indian Ocean to intraseasonal westerly winds (Sengupta et al. 2007).

5 Governing mechanisms

5.1 Role of intraseasonal WWBs

In the tropical troposphere strong organized moist atmospheric convection is characterized by low values of OLR (Liebmann and Smith 1996). Eastward propagating OLR minima over the central and eastern EIO in association with the MJO (Madden and Julian 1972) and the summer monsoon (Sikka and Gadgil 1980; Goswami and Ajai Mohan 2001) show strong intraseasonal variability with periods of 10–60 days. The WWBs associated with the atmospheric heating to the east (Gill 1982) also show corresponding intraseasonal oscillations with the periods of 10–40 days. The evolution of both OLR and ZW along the equator and of ZC at the Equator, 90°E for two contrasting years 2005 and 2007 clearly demonstrates the role of the WWBs in the generation of the intraseasonal jets in the ZC field of the near-surface layer through local frictional coupling (Fig. 9). A striking contrast is clearly seen in the intraseasonal variability of ZW and OLR (short lived east of 70°E) between both the years. The occurrence of strong WWBs is more pronounced in number, duration and intensity during 2005 in comparison to 2007. This difference has produced a corresponding difference between both the years in the distribution of eastward flowing jets in the ZC field in terms of their number, duration and vertical extent. The excellent one-to-one correspondence between the ZW and ZC jets is distinctly seen like a mirror image during 2005 and 2007 although the ZC jets lag the WWBs by a few days as simulated by Senan et al. (2003) and Sengupta et al. (2007). In

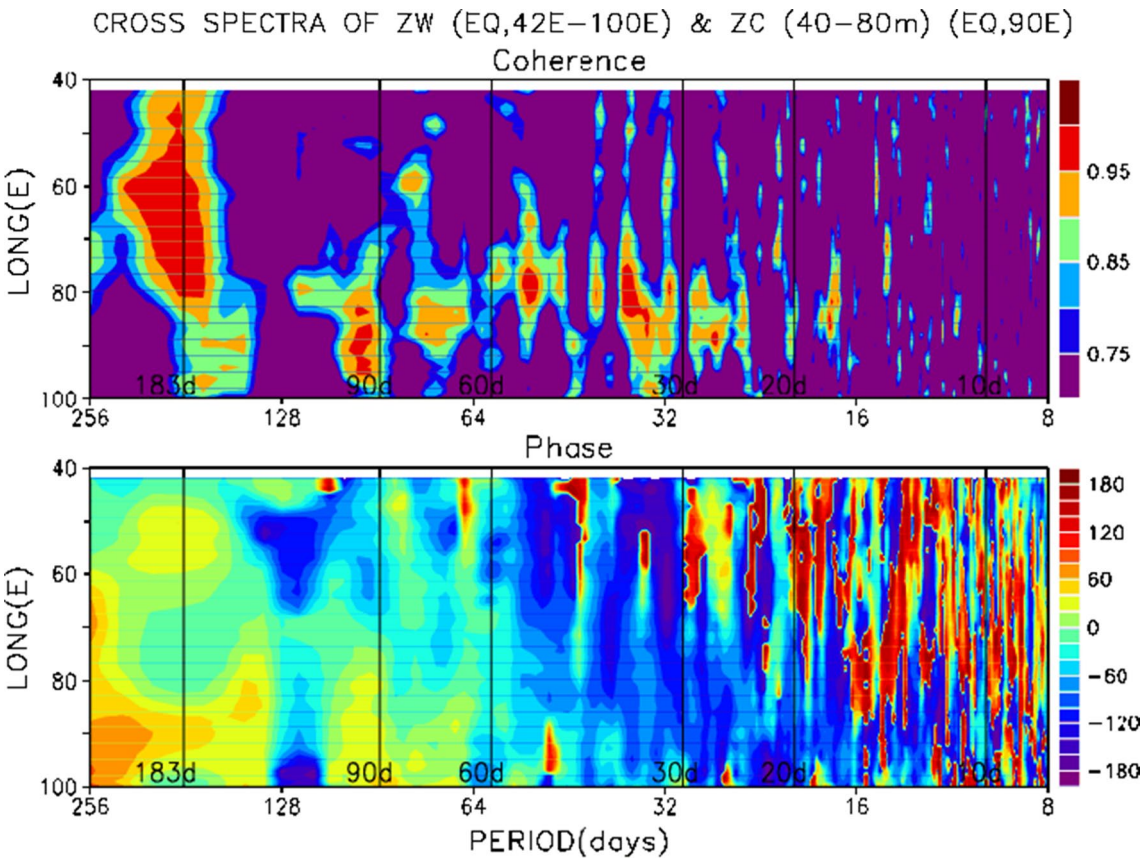

Fig. 10 Coherence (*top panel* in arbitrary units) and phase (*bottom panel* in degrees) between the ZC averaged over 40–80 m layer at the Equator, 90°E and the ZW along the equator. (*Vertical lines* indicate the most prominent periods for easy reference.)

general, similar features are also noticed during the other years of this observational study.

The cross spectra between the depth averaged near-surface (40–80 m) and subsurface (80–160 m) ZCs at the Equator, 90°E and the ZWs along the equator as coherence and phase are shown in Figs. 10 and 11 respectively. The coherence between near-surface ZCs and the equatorial ZWs is strongest at the semiannual period in the western and central EIO. This is in accordance with the earlier studies of Hase et al. (2008) and Iskandar et al. (2009). The phase difference of ZW variation at 60°E and the near-surface ZC variation at 90°E at the semiannual period is about 10 days. This indicates that the signal propagates eastward at about 3.8 m/s which is the speed of the eastward moving meteorological systems along the equator. In addition peaks at 41, 51 and at 95 day periods in the intraseasonal band are also noticed in the eastern EIO. On the other hand, the coherence between subsurface ZC and the equatorial ZWs is strongest at the semiannual period only in the western EIO (Fig. 11). The phase difference of ZW variation at 60°E and subsurface ZC variation at 90°E at the semiannual period is about 41 days. This indicates that the signal propagates eastward at about 0.93 m/s which may be a value between the characteristic speeds of the second and third baroclinic modes that is in general agreement with Iskandar et al. (2009) and Hase et al. (2008). There is also a suggestion of moderately strong coherence near 30 and 90 day periods in the eastern EIO.

5.2 Role of alongshore winds off the Somalia coast

In the northern (southern) hemisphere, alongshore winds with coastline to the right (left) excite coastal Kelvin waves that propagate along the coast (Gill 1982). The winds off the east coast of Somalia show a strong seasonal cycle. Northeasterlies (southwesterlies) blow during November–March (April–October; Rao et al. 2009a) favoring the excitation of downwelling (upwelling) coastal Kelvin waves north (south) of the equator off the Somalia coast (Izumo et al. 2008). Shankar et al. (2002) in their model simulation have carried out a sensitivity study to isolate the effect of the alongshore wind stress off the Somalia coast on the equatorial processes. They have found that the effect of the alongshore Somalia winds is felt in the EIO via the Kelvin wave propagation. The winds off the Somalia coast force strong local upwelling during the summer

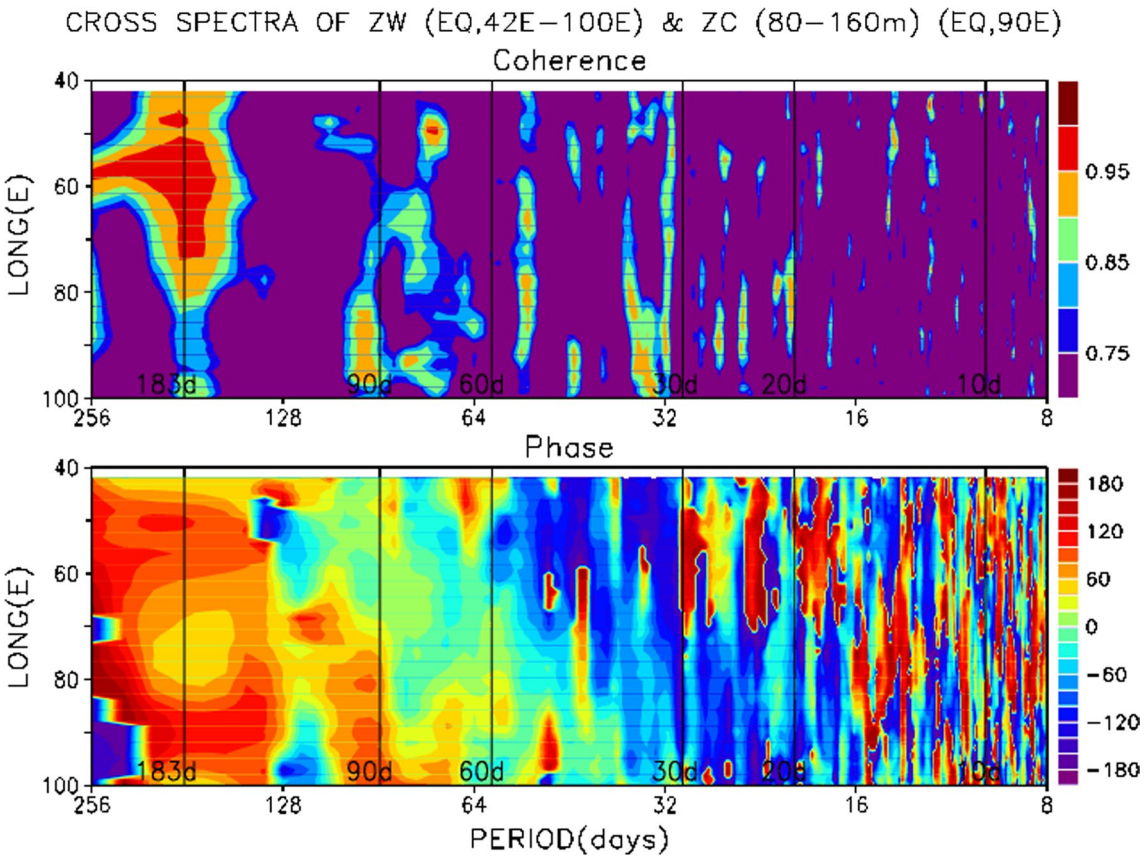

Fig. 11 Coherence (*top panel* in arbitrary units) and phase (*bottom panel* in degrees) between ZC averaged over 80–160 m layer at the Equator, 90°E and the ZW along the equator. (*Vertical lines* indicate the most prominent periods for easy reference.)

monsoon, and this signal is carried into the EIO, forcing a westward, upwelling-favourable equatorial current. This, together with the effect of the Rossby wave reflected from the coast of Sumatra in May, ensures a westward equatorial current during June–September in the eastern EIO and weakens the eastward current in the western EIO. This separates the eastward Summer Monsoon Current south of Sri Lanka from the westward flow at the equator. In another modeling study, Yuan and Han (2006) have shown that the alongshore winds off the Somalia coast and the Rossby waves in the off-equatorial regions contribute significantly to the annual harmonics of the equatorial Kelvin waves at the western boundary. The annual harmonic of the sea level remains large, producing a dominant annual oscillation of sea level in the central EIO. Thus, one would expect that these alongshore winds would significantly contribute to the evolution of the ZC field in the EIO on the annual mode. The observed alongshore winds off the Somalia coast within 2° of the equator with a primary focus during the preceding boreal winter are examined for the period of this study (Fig. 12). In general, bursts of northeasterly winds blow off the coastline during November–March, with significant differences among some years. These differences are in terms of total number of bursts, intensity and duration of their occurrence. Clearly the northeasterlies were less pronounced during the boreal winters of 2000–2001 and 2007–2008 in comparison to the rest of the winters. These differences in the surface wind forcing are expected to manifest their signatures in the annual mode of the zonal gradient of SSHA in the EIO and in the ZC field at the Equator, 90°E in the following year. Interestingly, the observed ZC field is also less pronounced during the following years, i.e. during both 2001 and 2008 (Fig. 5). Similarly the observed ZC field is more pronounced during the following years, i.e. during 2004, 2005 and 2007 when the alongshore winds are relatively stronger during the preceding boreal winters lending support to earlier modeling studies. Away from the western boundaries, instabilities cannot

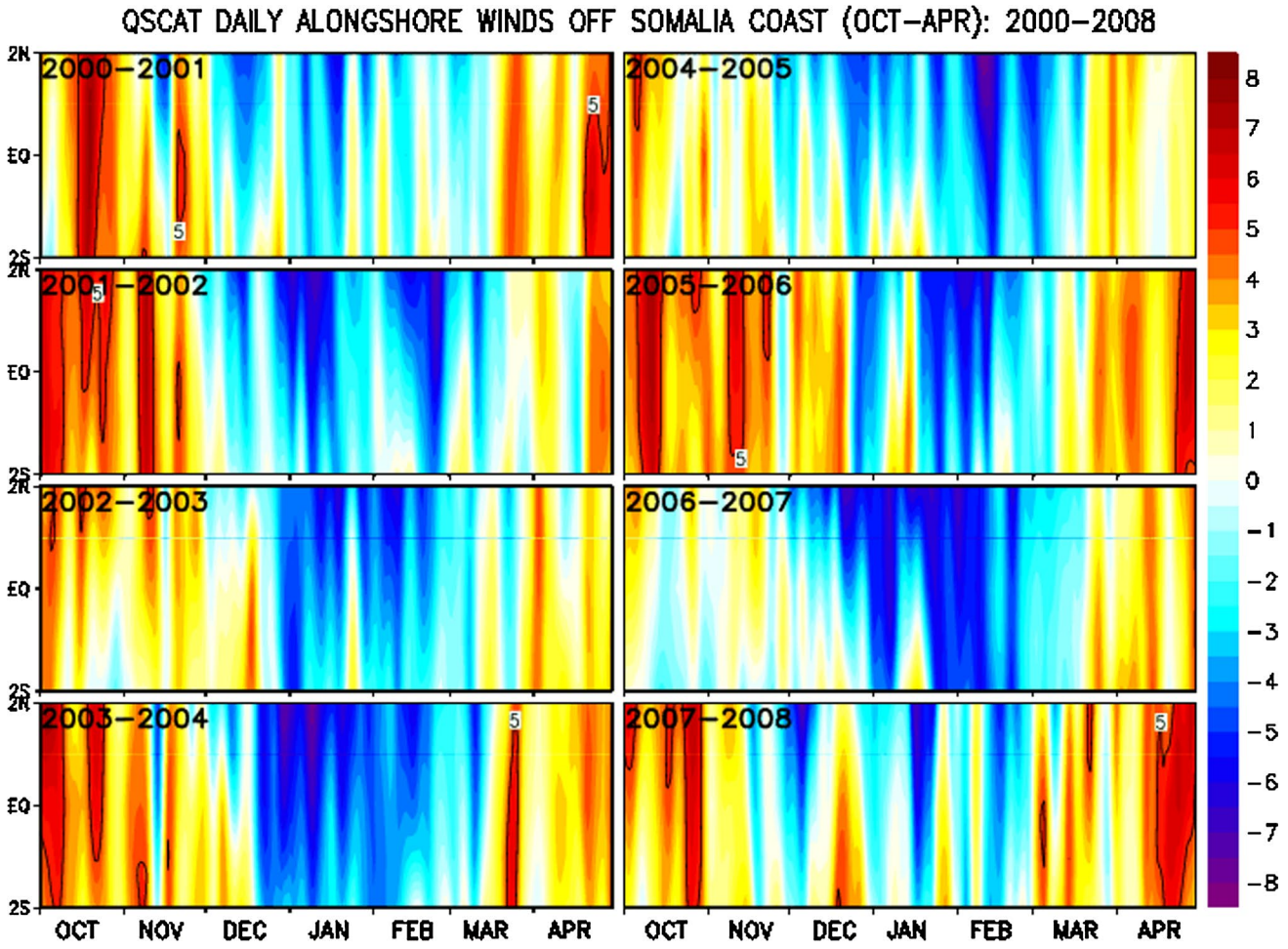

Fig. 12 Evolution of 3 day moving averages of QuikSCAT alongshore surface winds off the Somalia coast during October–April for the years 2000–2008

grow to large amplitude because their energy is rapidly removed by propagating waves (Philander 1990; Sengupta et al. 2001a).

5.3 Role of propagating waves

Recently Iskandar et al. (2009) and Rao et al. (2010) have shown that the annual cycle of eastward propagating Kelvin wave field in the equatorial waveguide of the TIO is composed of two pairs of alternate upwelling (first one occurring during January–March and the second one occurring during August–September) and downwelling (first one occurring during April–June and the second one occurring during October–December) waves. These waves produce horizontal variability in the ZPG field which influences the ZC field. The available long record of TRITON moored CTD data at 1.5°S and 90°E, permits to test this feature. The temporal evolution of vertical temperature and salinity fields of the uppermost 200 m water column at this location during 2001–2007 is shown in Fig. 13. In the thermocline the vertical oscillations of isotherms show a pronounced semiannual cycle. The salinity distribution also shows semiannual oscillation, with the occurrence of patches of subsurface maxima associated with the eastward flow originated in the Arabian Sea (Eriksen 1979; Hase et al. 2008). The relationship between the ZC variability and the isopycnal displacement is rather complex due to a mix of the semiannual and intraseasonal signals. In the surface layer, the eastward flowing ZCs associated with the intraseasonal Kelvin waves are accompanied with the downward isopycnal movements, showing the typical Kelvin wave responses. On the other hand, the eastward flowing ZCs in the pycnocline layer between 70 and 150 m depths do not show clear in-phase relation with isopycnal displacement. This is probably due to contamination of the semiannual signal of the reflected Rossby wave, as mentioned in Iskandar et al. (2009). The co-evolution of the ZC field and the isopycnals in the pycnocline shown in Fig. 13 supports the importance of the equatorial wave dynamics on the variability in the ZC and pycnocline displacement, which is first identified by the modeling studies.

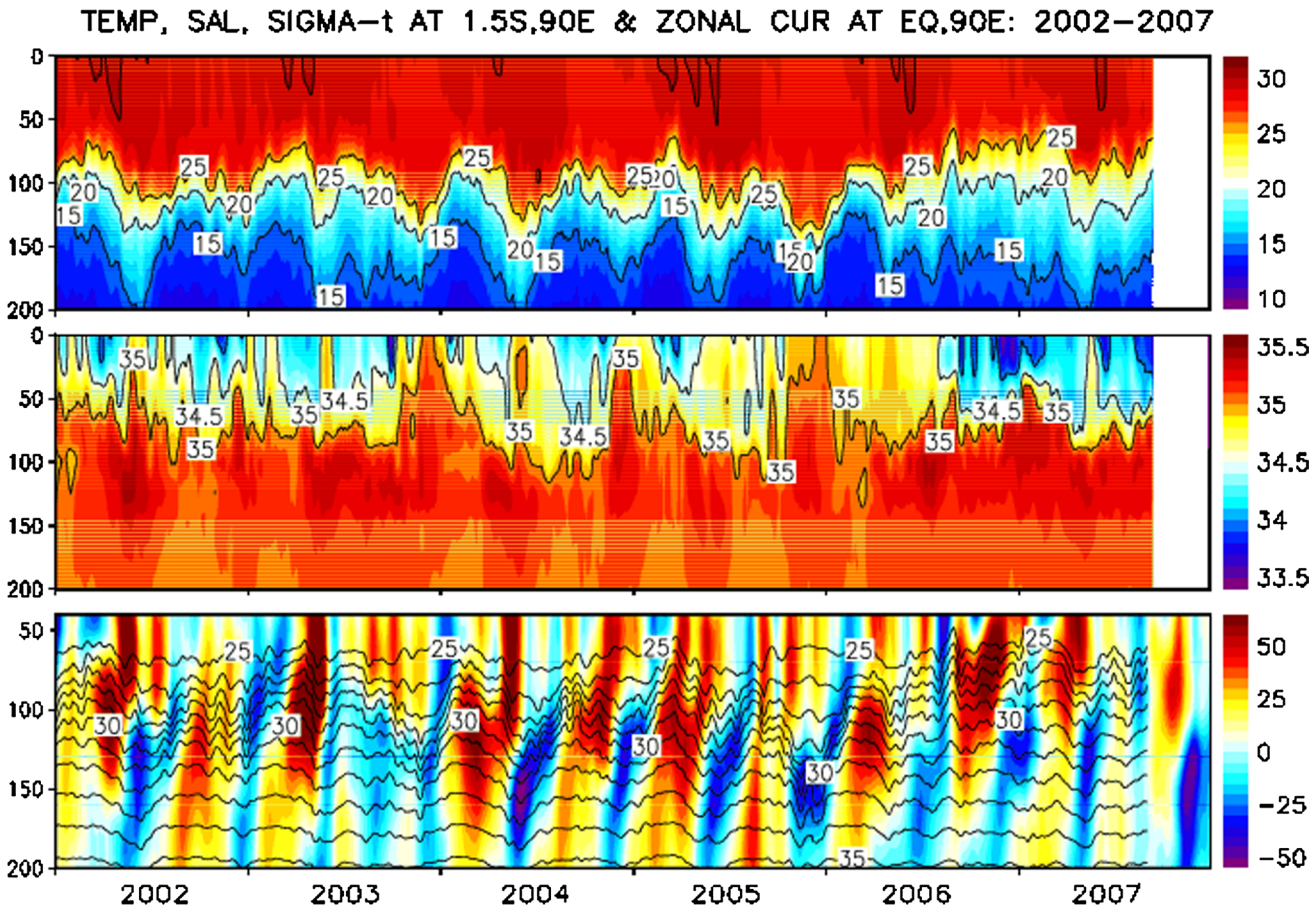

Fig. 13 Depth-time sections of temperature (°C) (*top panel*), salinity (PSU) (*middle panel*) at 1.5°S, 90°E in the upper most 200 m water column and ZCs (cm/s) at the Equator, 90°E in the 40–200 m water column with overlaid sigma-t contours (*bottom panel*) during 2002–2007

The concurrent time series measurements of ZCs made from two ADCP moorings co-located on the equator (at 90°E of JAMSTEC, Japan and at 80.5°E of PMEL, USA during the period 27 October, 2004–7 August, 2008) in the Indian Ocean have provided a unique observational framework to test the results of numerical modeling studies and satellite altimetry measurements that show the signatures of eastward propagating Kelvin waves in the equatorial wave guide forced by the surface ZW field. The cross spectra of ZCs recorded in the depth range of 40–160 m at these two sites as coherence and phase are shown in Fig. 14. In general the coherence between these two records is strong at the semiannual period throughout the depth range of 40–160 m with the strongest values occurring around 140 and 60 m depths. At intraseasonal periods (30–60 days) the coherence is limited to the near-surface layers only. At 140 m depth, the phase difference between both the records of about 6 days (signal lags at 90°E) suggests eastward propagation speed of the signal of about 2 m/s in close agreement with the phase speed of the baroclinic mode equatorial oceanic Kelvin waves (probably 2 m/s is the phase speed just between the first and second baroclinic modes). The speed of the Kelvin wave in the sea level data derived from AVISO SSHA is 2 m/s to the east (Le Blanc and Boulanger 2001). At 60 m depth, large coherence is noticed between the ZCs at 80.5°E and 90°E at 60 day period. The signal at 80.5°E leads that at 90°E with a phase difference of 6.6 days translates into propagation speed of about 1.83 m/s which broadly agrees with the eastward propagation speed of the Kelvin wave along the equator.

5.4 Role of ZPG

During boreal winter, the generation of eastward pressure gradient which drives an eastward flow in the thermocline, is caused primarily by upwelling equatorial Kelvin waves excited by prevailing easterly winds. On the other hand, the downwelling Rossby waves generated by the reflection of the spring downwelling Kelvin waves by the eastern boundary, as well as the upwelling equatorial Kelvin waves triggered by easterlies, create an oceanic state that favors the generation of the eastward pressure gradient during boreal summer (Iskandar et al. 2009). Senan et al. (2003) have shown close agreement between the zonal gradients of dynamic height from an OGCM simulation and SSHA for this region. In the absence of reliable and

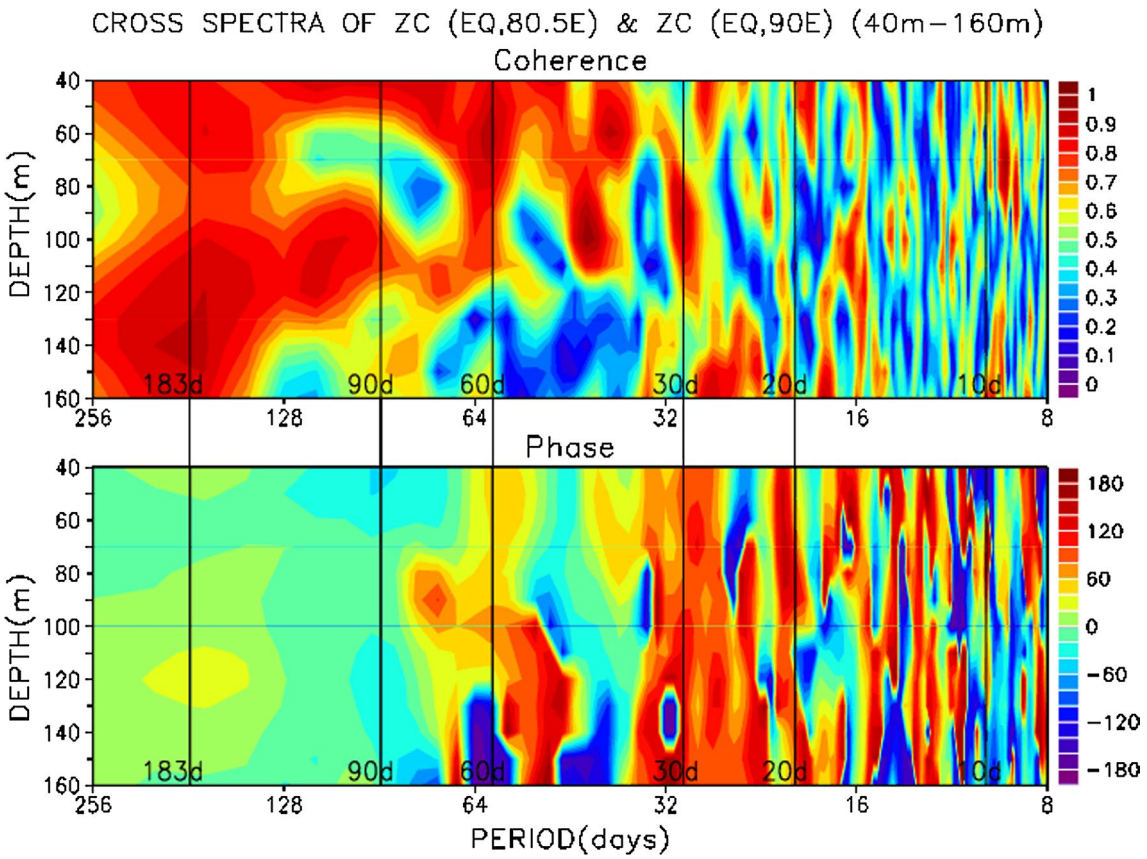

Fig. 14 Coherence (*top panel* in arbitrary units) and phase (*bottom panel* in degrees) between ZC over 40–160 m water column at the Equator, 90°E and the ZC over 40–160 m water column at the Equator, 80.5°E. (*Vertical lines* indicate the most prominent periods for easy reference.)

sufficient data on dynamic height derived from direct measurements of temperature and salinity profiles prior to 2004 from ARGO, the zonal gradient of SSHA along the equator is estimated from the averaged values of SSHA over two boxes in the west and east to represent ZPG. The choice of geographic locations for these two boxes was made based on the geographic location of spectral peaks of the SSHA close to the western and eastern rims shown in Fig. 8. The distribution of annual cycles of zonal gradient of SSHA in the EIO and the ZC of the subsurface layer at the Equator, 90°E for two contrasting years 2001 and 2004 is shown in Fig. 15. Both the parameters show a clear semiannual cycle with their peaks occurring with a phase difference of about 1 month—the time Kelvin waves take to propagate from the western rim to the eastern rim in the EIO. Interestingly both the years 2001 (weak) and 2004 (strong) show large differences in the amplitudes of the zonal SSHA gradient and ZC in tune with the corresponding differences in the amplitude of the alongshore winds during the respective preceding winters off the Somalia coast.

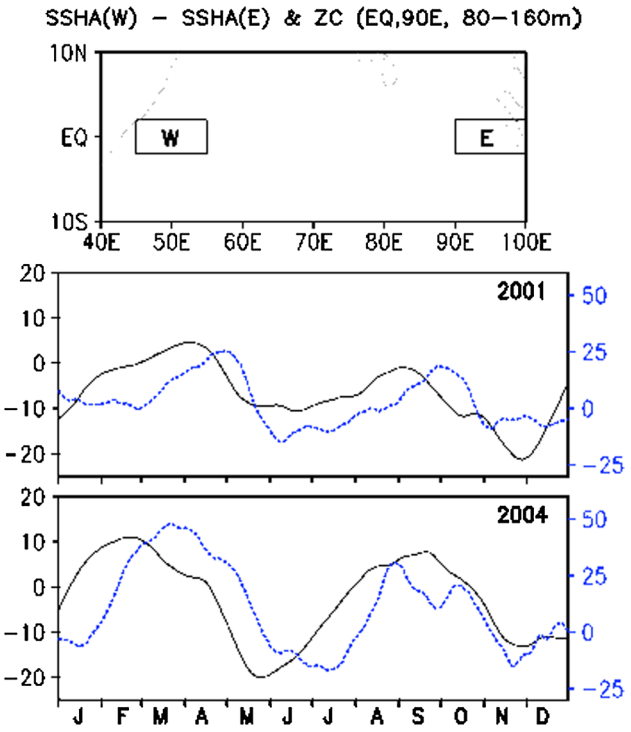

Fig. 15 31 day moving averages of zonal gradient of AVISO SSHA (cm) (*black lines*) between the western EIO (2°S–2°N, 45°E–55°E) and the eastern EIO (2°S–2°N, 90°E–100°E) (shown in the *top panel*) and ZC (cm/s) (*blue lines*) at the Equator, 90°E (80–160 m) during two contrasting years 2001 (*middle panel*) and 2004 (*bottom panel*)

5.5 Role of near-surface stratification

The role of near-surface salinity structure in the definition and dynamics of the mixed layer is increasingly recognized in the recent years. In a model simulation, in the eastern EIO, occurrence of rainfall during summer monsoon and boreal fall strengthens the boreal fall WJ due to thinning of the mixed layer in association with the salinity induced near-surface stratification (Han et al. 1999). Masson et al. (2002) have examined the seasonal variability and the formation mechanisms of the barrier layer in the eastern EIO from a 15 year OPA OGCM model simulation. They have found that the eastward advection of warm salty water by the WJ down to about 100 m and the northward advection of low salinity waters at the surface play an important role in the formation of the barrier layer. In another OGCM simulation, Masson et al. (2004) have shown the contribution of salinity induced stratification on the boreal fall WJ dynamics. The results of these modeling studies can be validated by combining the ADCP current measurements made at the Equator, 90°E and the vertical temperature and salinity profiles made by the TRITON CTD mooring at a nearby location 1.5°S, 90°E. Utilising both the temperature and salinity profiles the BLT is estimated following Lukas and Lindstorm (1991) and Sprintall and Tomczak (1992). The time series of observed ZC averaged over the near-surface (40–80 m) layer and the estimated BLT are shown for the years 2002–2007 (Fig. 16). The BLT shows strong seasonality with its minimum values occurring during February–March when the ZC field is relatively devoid of jets. During this period, in addition to the absence of WWBs low values of BLT also contribute to the absence of strong ZCs. The large values of BLT during the boreal spring and the summer monsoon season further help the WWBs to produce strong jets in the near-surface ZC field. The time series of 30–60 day bandpass filtered ZC averaged over 40–80 m depth and the BLT are shown for the years 2002–2007 in Fig. 17. In general, the temporal correspondence of these two time series both in amplitude and in phase is quite high indicating a strong relationship between the two. The ZC lags the BLT by about 4–5 days suggesting that this is the response time for the ZCs to build up under the ZW forcing when the mixed layer thins due to increase in BLT. Han et al. (1999) have indicated that the vertical shear of the ZC above the thermocline associated with the BLT further strengthens the surface jets owing to the trapping of momentum into the surface mixed layer.

The scatter between the 30 and 60 day bandpass filtered BLT and ZC averaged over 40–80 m water column is

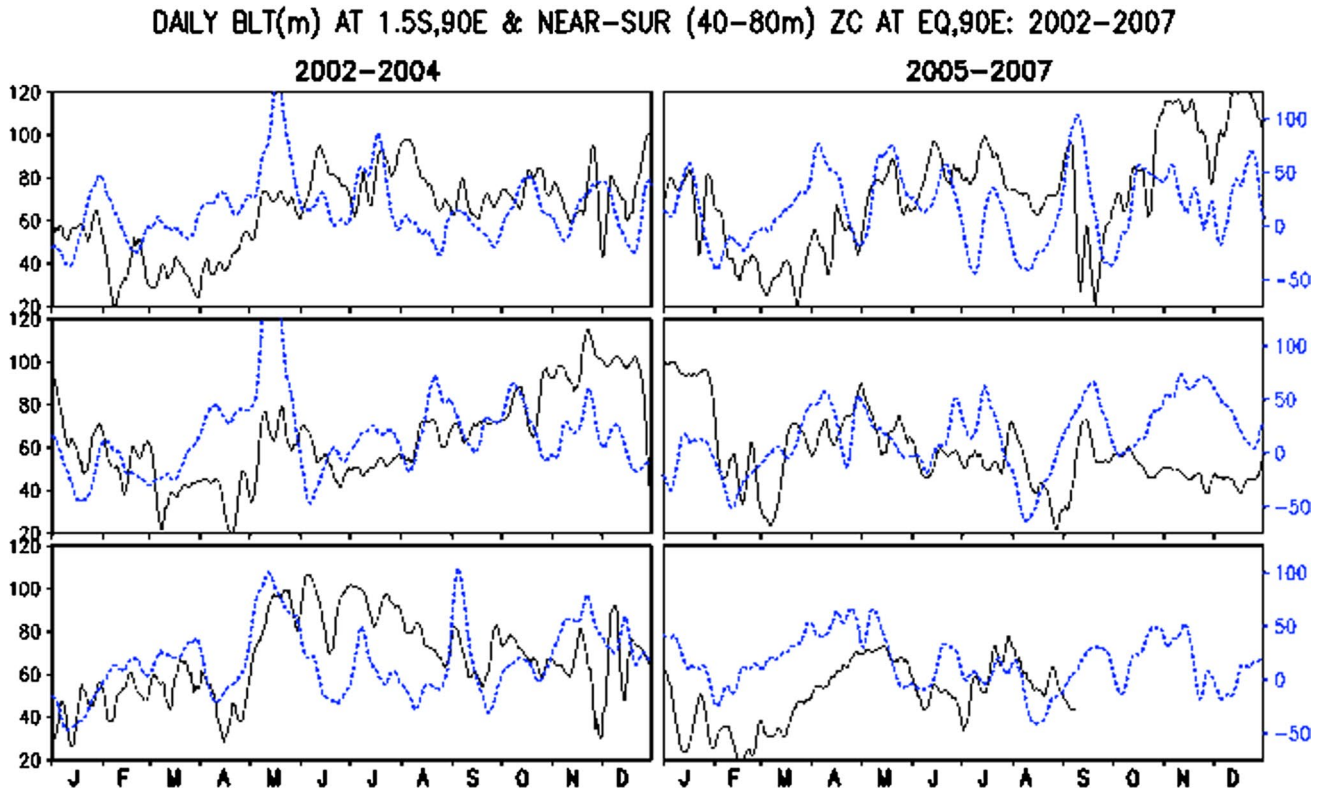

Fig. 16 Daily evolution of vertically averaged ZC (cm/s) (40–80 m) at the Equator, 90°E (*blue dashed line*) and BLT (m) at 1.5°S, 90°E (*black line*) during 2002–2007 (years increasing *downward in the vertical panels*)

shown in Fig. 18 for boreal spring and boreal fall months and the rest of the months in a year. Clearly an elliptical distribution suggests a strong relationship between BLT and ZC during both the monsoon transition months with a positive correlation coefficient of 0.57. On the other hand the relationship between these two is weak during the rest of the months in a year. The cross spectra between BLT and ZC averaged over 40–80 m layer is shown in Fig. 19. The coherence between BLT and ZC is quite pronounced at the semiannual period. In addition, strong peaks also occur in the temporal range of 30–60 days. The phase difference corresponding to the semiannual period suggests that the ZC builds up due to thinning of mixed layer due to increase in BLT in about a month's time.

6 Relationship with SST

In regions of warm SST and strong atmospheric convective activity such as the eastern EIO, small variations in SST can have significant impact on the interactions between the ocean and atmosphere. The SST of the eastern EIO is potentially affected by the WJs, which strongly deepen the thermocline by about 100 m associated with the presence of the barrier layer (Murtugudde and Busalacchi 1999; Masson et al. 2002). The zonal evolution of the observed annual cycle of the TRMM TMI SST (>29 °C) along the equator during the years 2001–2008 is presented in Fig. 20. In general, the distributions show semiannual variability with large (moderate) amplitude in the western (central and eastern) EIO. The strong cooling associated with both the boreal summer and boreal winter monsoons contribute to large semiannual variability in the westernmost region. The spring SST maxima (>29 °C) encompassing the central and the eastern EIO is the most pronounced signal during all the years. Similar to OLR and WWBs, intraseasonal oscillations are also seen in the evolution of SST almost throughout the year in the central and eastern EIO. The oscillations in these three fields are intimately coupled with each other through strong air-sea interaction processes (Sengupta et al. 2001b). The most striking feature of these distributions is the weak spring warming during the years 2008 and 2001—the surface expressions of the years of relatively weak ZC field. It is hypothesized that these anomalous weak heating patterns are likely to result from anomalous wave induced themocline/mixed layer depth distributions and the surface net air-sea heat flux forcings. Recently Rao et al. (2010) have shown large interannual variability in the eastward propagating Kelvin waves in the EIO. Their analysis has also indicated that the boreal spring Kelvin wave

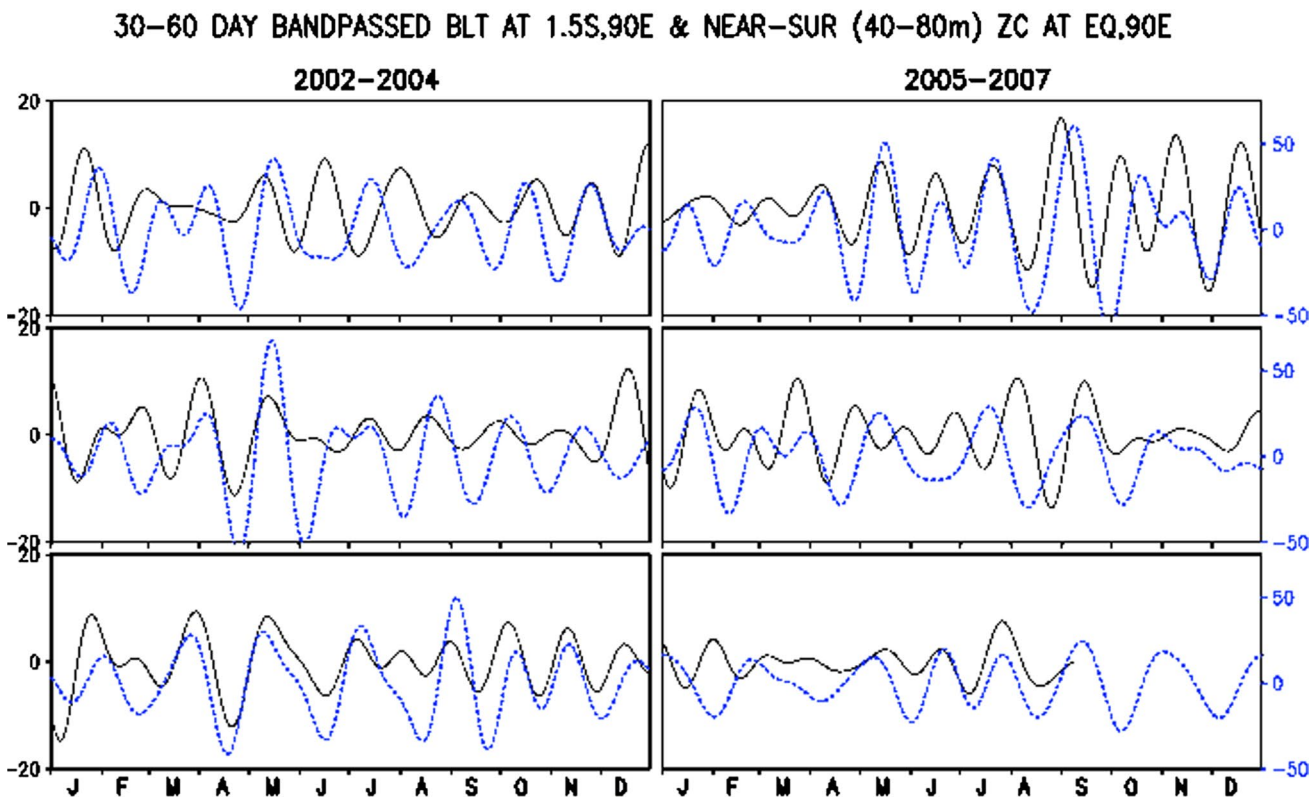

Fig. 17 Daily evolution of 30–60 day bandpass filtered *vertically* averaged ZC (cm/s) (40–80 m) at the Equator, 90°E (*blue line*) and BLT (m) at 1.5°S, 90°E (*black line*) during 2002–2007 (years increasing *downward in the vertical panels*)

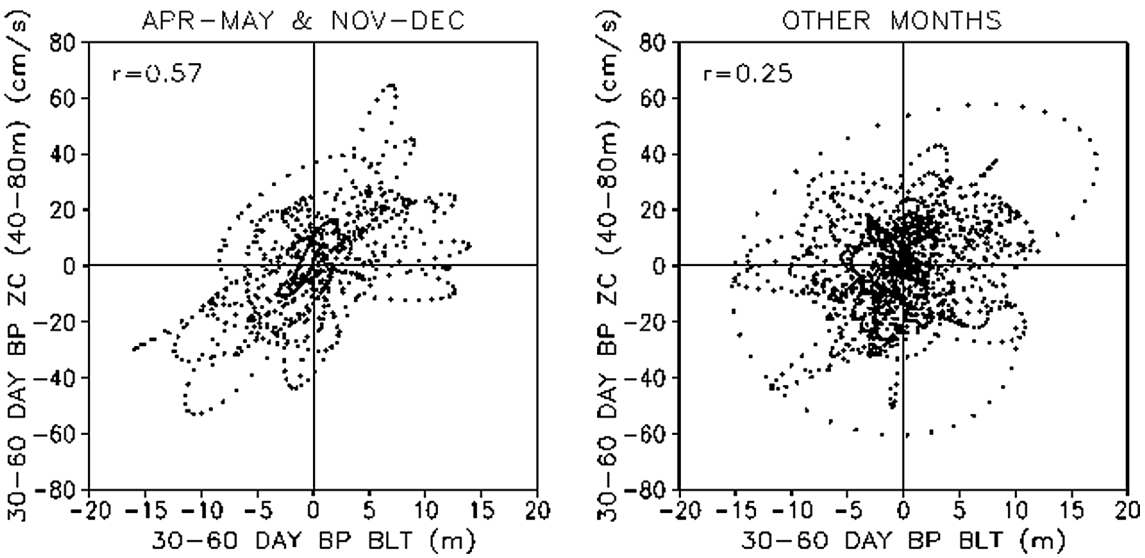

Fig. 18 Scatter plots between 30 and 60 day bandpass filtered BLT and ZC averaged over 40–80 m water column for monsoon transition months (*left panel*) and other months (*right panel*)

during 2001 is less pronounced than that of during 2004. It is therefore quite likely that the mixed layer depth and thermocline during the boreal springs of 2008 and 2001 are shallower than those of during any other year of strong SST maxima during boreal spring resulting in weaker heating of the mixed layer due to greater penetration of solar radiation

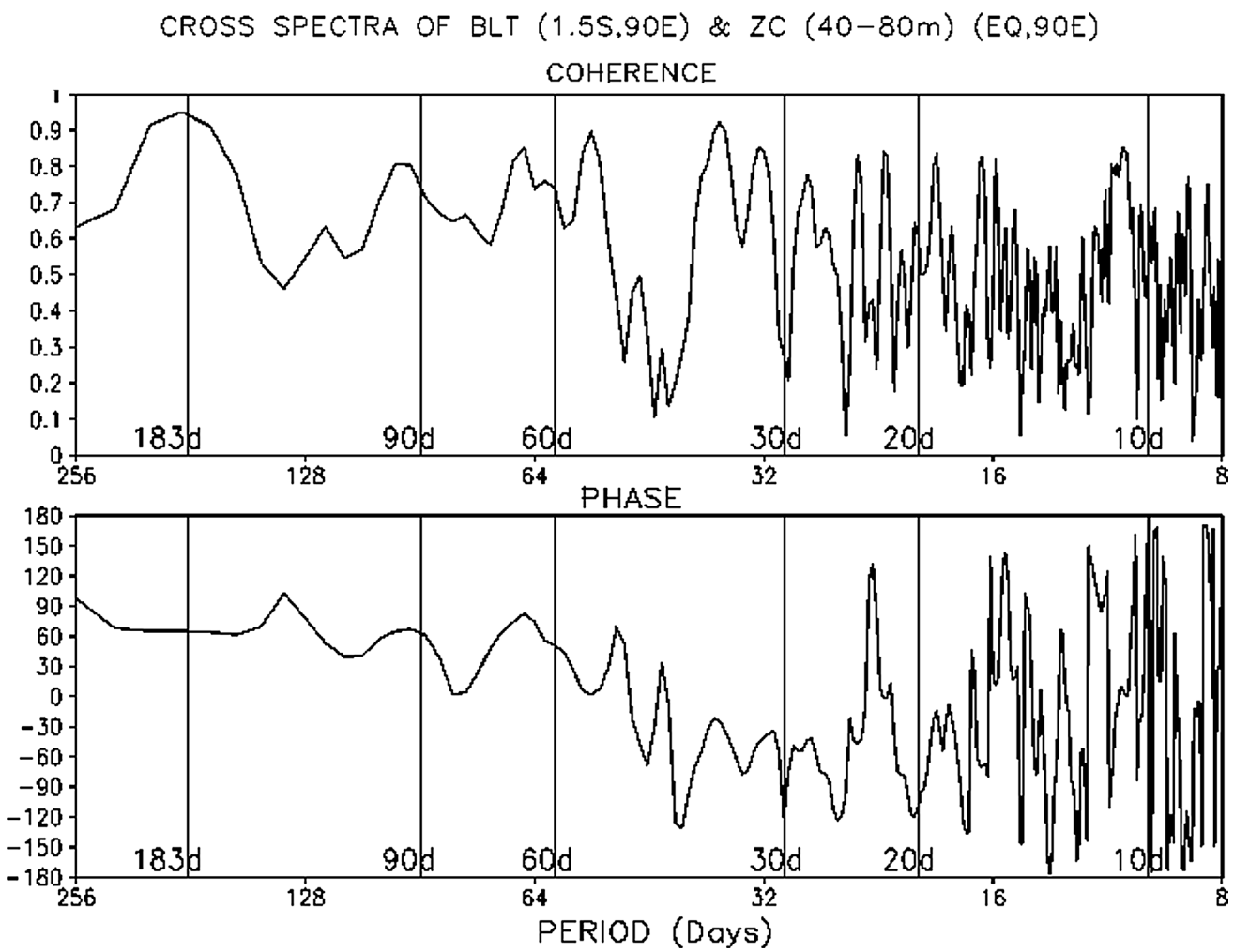

Fig. 19 Coherence (*top panel* in arbitrary units) and phase (*bottom panel* in degrees) between BLT at 1.5S, 90E and ZC (40–80 m) at Equator, 90E (*vertical lines* indicate the most prominent periods for easy reference.)

beneath the shallow mixed layer base—a process very much applicable to the warm pool regions in the tropical oceans (Vialard and Delecluse 1998a, b; Rao and Sivakumar 1999, 2000; Sengupta et al. 2002, 2008). Conversely, a downwelling Kelvin wave travelling along the equator will depress the thermocline; consequently the mixed layer becomes deeper and an anomalously warm surface layer is formed. Hence changes in SST are also indicative of vertical motions of the thermocline, which in turn can be related to the motion of the propagating waves in the equatorial wave guide.

In order to justify this speculation, the daily evolution of estimated WHOI surface net heat flux of Yu et al. (2008) along the equator is shown for two contrasting years 2001 and 2004 (Fig. 21). The distribution of surface net heat flux shows striking differences that are not in tune with the corresponding observed differences in the SST fields. This clearly suggests that although the surface net heat flux is larger during January–April 2001 in comparison to that of 2004, the spring SST of 2001 is relatively cooler than that of 2004 due to shallow mixed layer caused by weak Kelvin wave activity resulting in greater penetration of insolation beneath the shallow mixed layer base. However, the availability of limited number of ARGO temperature profiles before 2003 providing incomplete descriptions of mixed layer depth field along the equator and the non-availability of surface net heat flux data for 2008 do not permit to make a meaningful mixed layer heat budget analysis to resolve this issue at present. In addition, the unusual occurrence of WWBs during January–March also contribute to anomalous boreal spring heating in 2001 and 2008. The heat budget of the mixed layer for the contrasting years will be examined in detail in a separate study subsequently when the surface net heat flux data set for 2008 is available.

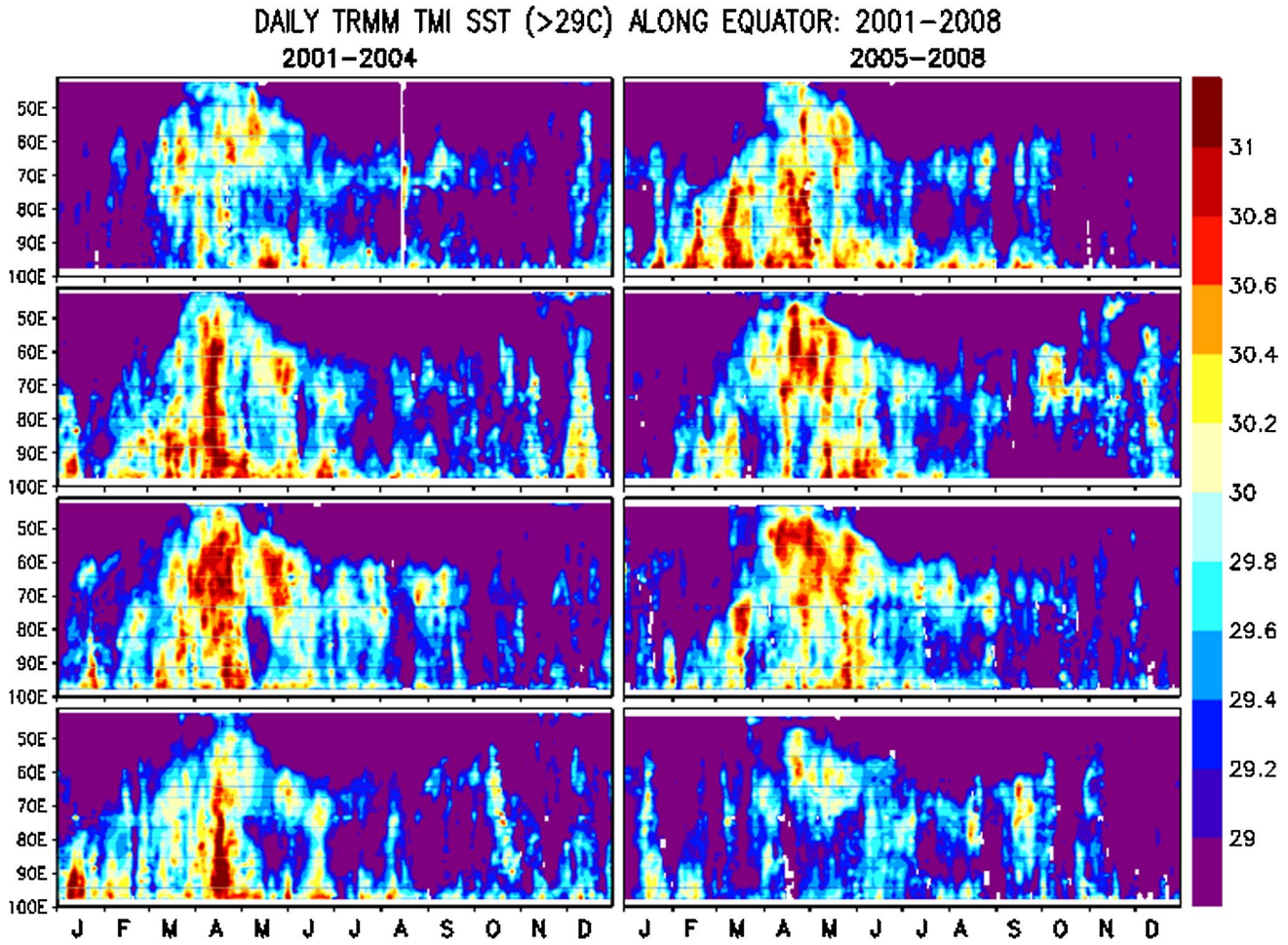

Fig. 20 Daily evolution of TRMM TMI SST (>29 °C) along the equator (averaged over 2°N–2°S) during 2001–2008 (years increasing downward in the *vertical panels*)

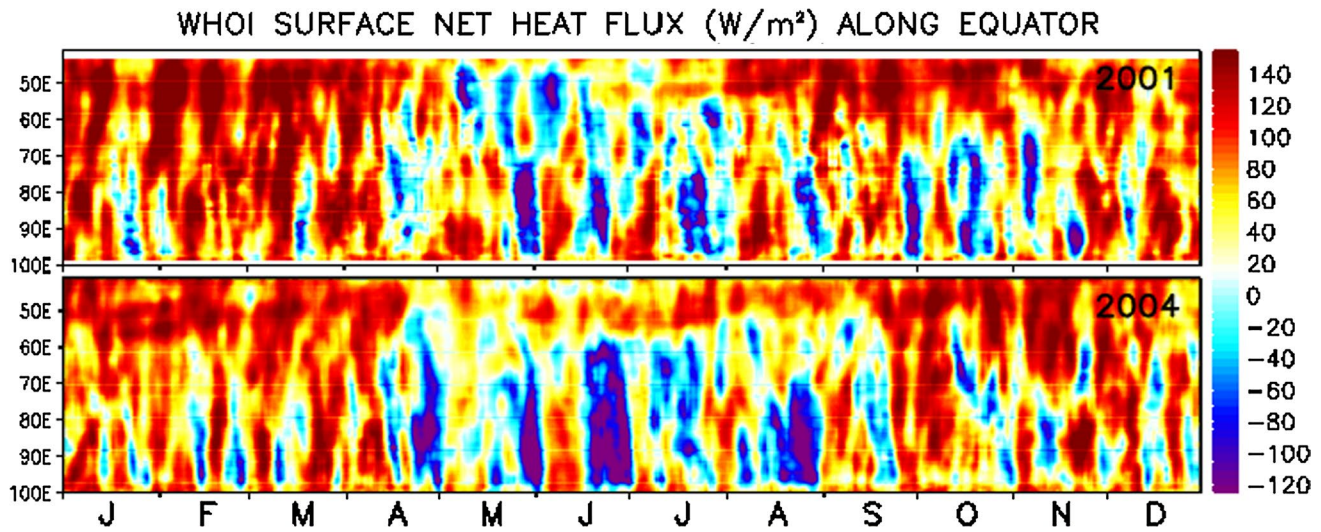

Fig. 21 Daily evolution of WHOI surface net heat flux (W/m^2) along the equator (averaged over 2°N–2°S) for the years 2001 and 2004

7 Summary and conclusions

On the basin scale, the ZWs show a strong semiannual signal in the western EIO a little away from the Somalia coast. On the intraseasonal mode the signal shifts to central and eastern EIO where the core of the warm pool is located. The signatures of the semiannual signal in respect of SSHA and D20 are pronounced in the north and south in the western EIO caused by the westward propagating Rossby waves and their boundary reflections. The ZC shows strong signals confining to the equator and near-equatorial regions at all the temporal modes. The observed annual cycle of the surface ZW climatology along the equator shows a strong semiannual mode with embedded intraseasonal oscillations on time scales of 10–40 day periods peaking during the transitions between both the monsoons. The variance of these westerly ZWs is larger over the eastern EIO. The intraseasonal WWBs show a strong semiannual cycle with peaks occurring during both the monsoon transitions and summer monsoon season only during some years. The ZCs between 40 and 350 m depths at the Equator, 90°E show periodic east–west reversals pronounced at the semiannual frequency with upward phase propagation suggesting the influence of eastward propagating Kelvin waves. In the near-surface layer, the ZC mostly flows eastward with occasional intensification occurring on intraseasonal time scale during April–July and September–December. The EUC is most pronounced in the depth range of 80–160 m during March–April and October–November. The direction and intensity of the flow in the near-surface layer are controlled by the prevailing ZWs through local frictional coupling. On the other hand the direction and intensity of the flow in the subsurface layer are determined by the ZPG set up by both surface ZW field and the propagating Kelvin and Rossby waves in the equatorial wave guide. In general, the ZC field is relatively weaker during 2001 and 2008 in comparison to the rest of the years. Although the SSHA field is relatively weaker during 2001 corresponding to a weaker ZC field, interestingly such a correspondence is not seen during 2008 for reasons unclear. All the parameters such as OLR, ZW and SSHA show strong semiannual signal in the EIO with their maxima occurring at different locations along the equator. In response, the ZC also shows a strong semiannual signal in the depth range of 80–160 m where the core of the EUC is located. Spectral peaks at 10–60 day intraseasonal periods are also seen in OLR, ZW and ZC, while the ZC also shows an additional peak at 90 days due to resonant excitation of the second baroclinic mode waves forced by the 90 day winds.

The role of the zonal WWBs driven by the tropospheric heating caused by organized moist convection in generating the jets in the ZC field through local frictional coupling is shown with examples for two contrasting years 2005 and 2007. The coherence between the near-surface (40–80 m) ZCs and the equatorial ZWs is strongest at the semiannual period in the western and central EIO. On the intraseasonal band, it is relatively more pronounced in the eastern EIO. On the other hand the coherence between the subsurface (80–160 m) ZC and the equatorial ZWs is strongest at the semiannual period in the western EIO. The examination of alongshore winds off the Somalia coast during the preceding boreal winter has shown an excellent relationship with the evolution of the ZC field at the Equator, 90°E in the following years. In agreement with the earlier modeling results, during the boreal winter transitions of 2000–2001 and 2007–2008, relatively weaker alongshore winds off the Somalia coast have contributed to relatively weaker ZC field during 2001 and 2008. It can be hypothesized that stronger (weaker) alongshore winds off the Somalia coast drive stronger (weaker) coastal Kelvin waves that propagate along the wave guide of the equator of the EIO, set up stronger (weaker) ZPG resulting in a stronger (weaker) ZC field.

In the pycnocline the vertical oscillations show a pronounced semiannual mode in tune with the propagating Kelvin waves throughout the record. The co-evolution of the ZC field at the Equator, 90°E and the isopycnals derived from the temperature and salinity fields in the pycnocline at a nearby TRITON CTD mooring (1.5°S, 90°E) shows strong association of eastward (westward) flow with downwelling (upwelling) regime consistently throughout the record lending support to the influence of propagating Kelvin waves on the ZC field. The concurrent time series measurements of ZCs on the equator at 80.5°E and 90°E have shown the eastward propagation of baroclinic Kelvin waves with a speed of 2 m/s.

A nearby TRITON CTD mooring data have shown the evolution of BLT with rich seasonality. The annual cycle of BLT shows minimum values during February–March when the jets in the ZC field are also absent. The large values of BLT during the boreal spring and the summer monsoon further help the WWBs to trigger jets in the near-surface ZC field. On intraseasonal time scale, the response time for the buildup of ZCs due to trapping of zonal momentum into a thinning mixed layer appears to be about 4–5 days. The evolution of the Kelvin waves also appears to influence the seasonal evolution of SST along the equator. For instance, in tune with the observed weak ZC field, the SST also showed weak surface expressions during the boreal spring seasons of 2001 and of 2008. A close examination of the available surface net heat flux however, does not justify such a strong contrast between the years 2001 and 2004 suggesting the possible role played by the shoaling of the mixed layer and the thermocline caused by a weak Kelvin wave activity resulting in increased penetration of insolation beneath the shallow mixed layer base during 2001. A detailed heat budget analysis of the mixed layer in the EIO is necessary to resolve this issue. In general the availability of recent high

resolution satellite measurements have played a critical role in our current understanding of the dynamics of the ZC in the EIO. Future analysis of long time series measurements made through the deployment of moored vertical arrays in their full measure under RAMA observational initiative in the TIO and improved models would provide answers to questions that remained unanswered in this study.

Acknowledgments Highest appreciation is placed on record for the excellent compilation by several persons and organizations of all the data sets utilized in this study. The JAMSTEC is responsible for the deployment of ADCP and TRITON CTD moorings in the eastern EIO. The PMEL is responsible for the deployment of ADCP moorings in the central EIO. The authors are grateful to Dr M. S. Girishkumar for his help with the alongshore winds off the Somalia coast. The authors thank Prof D. Sengupta for bringing the OAFlux data to their attention. The Graphics are generated with GrADS. The encouragement and the facilities provided by the Director General, JAMSTEC are gratefully appreciated. This research was carried out while the first author held a Visiting Senior Scientist position at JAMSTEC with the support of JEPP (Japan Earth Observation Promotion Program) of MEXT (Ministry of Education, Culture, Sports, Science & Technology), Japan.

References

Akima H (1970) A new method of interpolation and smooth curve fitting based on local procedures. J Assoc Comput Mech 17:589–602

Anderson DLT, Carrington DJ (1993) Modeling interannual variability in the Indian Ocean using momentum fluxes from the operational weather analysis of the United Kingdom Meteorological Office and European Centre for Medium-Range Weather Forecasts. J Geophys Res 98:12483–12499

Basu S, Meyers SD, O'Brien JJ (2000) Annual and interannual sea level variations in the Indian Ocean from TOPEX/Poseidon observations and ocean model simulations. J Geophys Res 105(C1):975–994

Brandt P, Stramma L, Schott F, Fischer J, Dengler M, Quadfasel D (2002) Annual Rossby waves in the Arabian Sea from TOPEX/POSEIDON altimeter and in situ data. Deep-Sea Res II 49:1197–1210

Bubnov VA (1994) Climatic zonal pressure gradient in the equatorial zone of the Indian Ocean. Oceanology 33:414–420

Cane M (1980) On the dynamics of equatorial currents, with application to the Indian Ocean. Deep-Sea Res 27A:525–544

Cane M, Moore DW (1981) A note on low frequency equatorial basin modes. J Phys Oceangr 11:1578–1584

Cutler AN, Swallow JC (1984) Surface currents in the Indian Ocean (to 25°S, 100°E): compiled from historic data archived by the Meteorological Office, Institute of Ocean Sciences, Wormly, UK, Rept. No. 187, 8 p and 36 charts

Duchon CE (1979) Lanczos filter in one and two dimensions. J Appl Meteorol 18:1016–1022

Eriksen CC (1979) An equatorial transect of the Indian Ocean. J Mar Res 37:215–232

Fu LL (2007) Intraseasonal variability of the equatorial Indian Ocean observed from sea surface height, wind, and temperature data. J Phys Oceanogr 37:188–202

Gent PR, O'Neill K, Cane MA (1983) A model of the semiannual oscillation in the equatorial Indian Ocean. J Phys Oceanogr 13:2148–2160

Gill AE (1982) Atmosphere-ocean dynamics, international geophysics series, vol 30. Academic Press, London **662 p**

Gnanaseelan C, Deshpande A, McPhaden MJ (2012) Impact of Indian Ocean Dipole and El Niño/Southern oscillation wind-forcing on the Wyrtki jets. J Geophys Res 117:C08005, 1–11. doi:10.1029/2012JC007918

Gordon AL, Susanto D, Huber BA, Sullstyo B, Supangat A (2009) Seven years of measuring the Makassar Strait throughflow—the primary component of the Indonesian Throughflow (unpublished manuscript)

Goswami BN, Ajai Mohan RS (2001) Intraseasonal oscillations and interannual variability of the Indian summer monsoon. J Clim 14:1180–1198

Goswami BN, Sengupta D (2003) A note on the deficiency of NCEP/NCAR reanalysis surface winds over the equatorial Indian Ocean. J Geophys Res 108:3124. doi:10.1029/2002JC001497

Grodsky SA, Carton J, Murtugudde R (2001) Anomalous surface currents in the tropical Indian Ocean. Geophys Res Lett 28:4207–4210

Han W (2005) Origins and dynamics of the 90-day and 30–60-day variations in the equatorial Indian Ocean. J Phys Oceanogr 35:708–728

Han W, McCreary JP, Anderson JDLT, Mariano AJ (1999) On the dynamics of the eastward surface jets in the equatorial Indian Ocean. J Phys Oceanogr 29:2191–2209

Han W, Lawrence DM, Webster PJ (2001) Dynamical response of equatorial Indian Ocean to intraseasonal winds: zonal flow. Geophys Res Lett 28:4215–4218

Han W, Webster PJ, Lukas R, Hacker P, Hu A (2004) Impact of atmospheric intraseasonal variability in the Indian Ocean: low-frequency rectification in equatorial surface current and transport. J Phys Oceanogr 34:1350–1372

Han W, Shinoda T, Fu LL, McCreary JP (2006) Impact of atmospheric intraseasonal oscillations on the Indian Ocean dipole during the 1990s. J Phys Oceanogr 36:670–690

Hase H, Masumoto Y, Kuroda Y, Mizuno K (2008) Semiannual variability in temperature and salinity observed by Triangle Transocean Buoy Network (TRITON) buoys in the eastern tropical Indian Ocean. J Geophys Res 113:C01016. doi:10.1029/2006JC004026

Hino M (1977) Spectral analysis. Published by Asakura-SyoTen, 300 p (in Japanese)

Hood R, Naqvi W, Wiggert J, Goes J, Coles V, McCreary JP, Bates N, Karuppasamy PK, Mahowald N, Seitzinger S, Meyers G (2008) Research opportunities and challenges in the Indian Ocean. EOS Trans AGU 89(13):125–126

Horii T, Hase H, Ueki I, Masumoto Y (2008) Oceanic precondition and evolution of the 2006 Indian Ocean Dipole. Geophys Res Lett 35:L03067. doi:10.1029/2007GL032464

Iskandar I, McPhaden MJ (2011) Dynamics of wind-forced intraseasonal zonal current variations in the equatorial Indian Ocean. J Geophys Res 116:C06019. doi:10.1029/2010JC006864

Iskandar I, Mardiansyah W, Masumoto Y, Yamagata T (2005) Intraseasonal Kelvin waves along the southern coast of Sumatra and Java. J Geophys Res 110:C04013. doi:10.1029/2004JC002508

Iskandar I, Tozuka T, Masumoto Y, Yamagata T (2008) Impact of Indian Ocean dipole on intraseasonal zonal currents at 90°E on the equator as revealed by the self-organizing map. Geophys Res Lett 35:L14S03. doi:10.1029/2008GL033468

Iskandar I, Masumoto Y, Mizuno K (2009) Subsurface equatorial zonal current in the eastern Indian Ocean. J Geophys Res 114:C06005. doi:10.1029/2008JC005188

Izumo T, de Boyer Montégut C, Luo J, Behera SK, Masson S, Yamagata T (2008) The role of the western Arabian Sea upwelling in Indian monsoon rainfall variability. J Clim 21:5603–5623

Jensen TG (1993) Equatorial variability and resonance in a wind-driven Indian Ocean model. J Geophys Res 98:22533–22552
Johnson ES, Bonjean F, Lagerloef GSE, Gunn JT, Mitchum GT (2007) Validation and error analysis of OSCAR sea surface currents. J Ocean Atmos Technol 24(4):688–701
KNMI (1952) Indische Ocean Oceanographische and Meteorologische gegevens, 2nd Ed. Publ. No. 135, I, 31 p and II, 24 charts
Knox R (1976) On a long series of measurements of Indian Ocean equatorial currents near Addu Atoll. Deep-Sea Res 23:211–221
Kuroda Y (2002) TRITON: present status and future plan. JAMSTEC Tech. Rep. TOCS 5, Japan Marine Science and Technology Center, Yokosuka, Japan, 77 p
Lagerloef GSE, Mitchum GT, Lukas R, Niiler PP (1999) Tropical Pacific near surface currents estimated from altimeter, wind and drifter data. J Geophys Res 104:23313–23326
Le Blanc J-L, Boulanger J-P (2001) Propagation and reflection of long equatorial waves in the Indian Ocean from TOPEX/POSEIDON data during the 1993–1998 period. Clim Dyn 17:547–557
Liebmann B, Smith CA (1996) Description of a complete (interpolated) OLR dataset. Bull Am Meterol Soc 77:1275–1277
Lukas R, Lindstorm E (1991) The mixed layer of the western equatorial Pacific Ocean. J Geophys Res 96:3343–3357
Luyten JR, Roemmich DH (1982) Equatorial currents at semiannual period in the Indian Ocean. J Phys Oceanogr 12:406–413
Madden RA, Julian PR (1972) Description of global-scale circulation cells in the tropics with a 40–50 day period. J Atmos Sci 29:1109–1123
Mariano AJ, Ryan H, Perkins BD, Smithers S (1995) The Mariano global surface velocity analysis 1.0, report no CG-D-34-95, U. S. Dept. of Transportation, Washington D.C., 20593-0001, 55 p
Masson S, Delecluse P, Boulanger J-P, Menkes C (2002) A model study of the seasonal variability and formation mechanisms of barrier layer in the eastern equatorial Indian Ocean. J Geophys Res 107:8017. doi:10.1029/2001JC000832
Masson S, Boulanger J-P, Menkes C, Delecluse P, Yamagata T (2004) Impacts of salinity on the 1997 Indian Ocean dipole event in a numerical experiment. J Geophys Res 109:C02002. doi:10.1029/2003JC001807
Masumoto Y, Meyers G (1998) Forced Rossby waves in the southern tropical Indian Ocean. J Geophys Res 103(C12):27589–27602
Masumoto Y, Hase H, Kuroda Y, Matsuura H, Takeuchi K (2005) Intraseasonal variability in the upper layer currents observed in the eastern equatorial Indian Ocean. Geophys Res Lett 32:L02607. doi:10.1029/2004GL021896
Masumoto Y, Horii T, Ueki I, Hase H, Ando K, Mizuno K (2008) Short-term upper ocean variability in the central equatorial Indian Ocean during 2006 Indian Ocean dipole event. Geophys Res Lett 35:L14S06. doi:10.1029/2008GL033834
McCreary JP, Kundu PK, Molinari RL (1993) A numerical investigation of dynamics, thermodynamics and mixed layer processes in the Indian Ocean. Prog Oceanogr 31:181–244
McPhaden MJ (1982) Variability in the central equatorial Indian Ocean: I. Ocean dynamics. J Mar Res 40:157–176
McPhaden MJ, Meyers G, Ando K, Masumoto Y, Murty VSN, Ravichandran M, Syamsudin F, Vialard J, Yu L, Yu W (2009) RAMA the research moored array for African–Asian–Australian monsoon analysis and prediction. Bull Am Meterol Soc 90:459–480. doi:10.1175/2008BAMS2608
Molinari R, Olson D, Reverdin G (1990) Surface current distributions in the tropical Indian Ocean derived from compilations of surface buoy trajectories. J Geophys Res 95(C5):7217–7238
Murtugudde R, Busalacchi AJ (1999) Interannual variability of the dynamics and thermodynamics of the tropical Indian Ocean. J Clim 12:2300–2326
Murty VSN, Sarma MSS, Suryanarayana A, Sengupta D, Unnikrishnan AS, Fernando V, Almeida A, Khalap S, Sardar A, Somasundar K, Ravichandran M (2006) Indian moorings; deep-sea current meter moorings in eastern equatorial Indian Ocean. *CLIVAR Exchanges*, No. 11(4), International CLIVAR Project Office, Southampton, United Kingdom, pp 5–8
Nagura M, McPhaden MJ (2008) The dynamics of zonal current variations in the central equatorial Indian Ocean. Geophys Res Lett 35:L23603. doi:10.1029/2008/GL035961
Nagura M, McPhaden MJ (2010a) Wyrtki Jet dynamics: seasonal variability. J Geophys Res 115:C07009. doi:10.1029/2009JC005922
Nagura M, McPhaden MJ (2010b) Dynamics of zonal current variations associated with the Indian Ocean dipole. J Geophys Res 115:C11026. doi:10.1029/2010JC006423
Nagura M, McPhaden MJ (2012) The dynamics of wind-driven intraseasonal variability in the equatorial Indian Ocean. J Geophys Res 117:C02001. doi:10.1029/2011JC007405
O'Brien JJ, Hurlburt HE (1974) Equatorial jet in the Indian Ocean: theory. Science 184:1075–1077
Philander SGH (1990) El Niño, La Niña and the Southern Oscillation. Academic Press, London **293 p**
Philander SGH, Pacanowski RC (1980) The generation of equatorial currents. J Geophys Res 85:1123–1136
Potemra JT, Luther ME, O'Brien JJ (1991) The seasonal circulation of the upper ocean in the Bay of Bengal. J Geophys Res 96:12667–12683
Rahul Chand Reddy P, Salvekar PS, Deo AA, Ganer GW (2004) Westward propagating twin gyres in the equatorial Indian Ocean. Geophys Res Lett 31:L01304. doi:10.1029/2003GL018615
Rao AS, Behera SK (2005) Subsurface influence on SST in the tropical Indian Ocean: structure and interannual variability. Dyn Atmos Ocean 39:103–135
Rao RR, Sivakumar R (1999) On the possible mechanisms of the evolution of a mini warm pool during the pre-summer monsoon season and the onset vortex in the southeastern Arabian Sea. Q J R Meterol Soc 125:787–809
Rao RR, Sivakumar R (2000) Seasonal variability of the heat budget of the mixed layer and the near-surface layer thermal structure of the tropical Indian Ocean from a new global ocean temperature climatology. J Geophys Res 105(C1):995–1015
Rao RR, Molinari RL, Festa JF (1991) Surface meteorological and subsurface oceanographic atlas of the tropical Indian Ocean, *NOAA Technical Memorandum, ERL AOML-69*, 59 p
Rao AS, Behera SK, Masomoto Y, Ymagata T (2002) Interannual subsurface variability in the tropical Indian Ocean with a special emphasis on the Indian Ocean Dipole. Deep Sea Res Part II 49:1549–1572
Rao RR, Girish Kumar MS, Ravichandran M, Satheesh Kumar S (2009a) Atlas of the tropical Indian Ocean from satellite observations, volume I: sea surface wind vectors and wind stress curl, Indian National Centre for Ocean Information Services (INCOIS), Hyderabad, India, 278 p. ISBN 978-81-8424-326-0
Rao RR, Girish Kumar MS, Ravichandran M, Satheesh Kumar S (2009b) Atlas of the tropical Indian Ocean from satellite observations, volume III: sea surface height anomalies and circulation, Indian National Centre for Ocean Information Services (INCOIS), Hyderabad, India, 207 p. ISBN 978-81-8424-326-0
Rao RR, Girish Kumar MS, Ravichandran M, Rao AR, Gopalakrishna VV, Thadathil P (2010) Interannual variability of Kelvin wave propagation in the wave guides of the equatorial Indian Ocean, the coastal Bay of Bengal and the southeastern Arabian Sea during 1993–2006. Deep-Sea Res I 57:1–13
Reppin J, Schott F, Fischer J, Quadfasel D (1999) Equatorial-currents and transports in the upper central Indian Ocean: annual cycle and interannual variability. J Geophys Res 104(C7):15495–15514

Reverdin G (1987) The upper equatorial Indian Ocean: the climatological seasonal cycle. J Phys Ocean 17:903–927

Reverdin G, Cadet DL, Gutzler D (1986) Interannual displacementsof convection and surface circulation over the equatorial Indian Ocean. Q J R Meteorol Soc 112:43–67

Saji NH, Goswami BN, Vinayachandran PN, Yamagata T (1999) A dipole mode in the tropical Indian Ocean. Nature 401:360–363

Schott F, McCreary JP (2001) The monsoon circulation of the Indian Ocean. Prog Oceanogr 51:1–123

Schott F, Reppin J, Fischer J, Quadfasel D (1994) Currents and transports of the monsoon current south of Sri Lanka. J Geophys Res 99:25127–25141

Schott FA, Xie SP, McCreary JP (2009) Indian Ocean circulation and climate variability. Rev Geophys 47:RG1002. doi:10.1029/2007RG000245

Schouten MW, de Ruijter WPM, van Leeuwen PJ, Dijkstra HA (2002) An oceanic teleconnection between the equatorial and southern Indian Ocean. Geophys Res Lett 29:1812. doi:10.1029/2001GL014542

Senan R, Sengupta D, Goswami BN (2003) Intraseasonal "monsoon jets" in the equatorial Indian Ocean. Geophys Res Lett 30:1750. doi:10.1029/2003GL017583

Sengupta D, Senan R, Goswami BN (2001a) Origin of intraseasonal variability of circulation in the tropical central Indian Ocean. Geophys Res Lett 28:1267–1270

Sengupta D, Goswami BN, Senan R (2001b) Coherent intraseasonal oscillations of ocean and atmosphere during the Asian summer monsoon. Geophys Res Lett 28(21):4127–4130

Sengupta D, Ray PK, Bhat GS (2002) Spring warming of the eastern Arabian Sea and Bay of Bengal from buoy data. Geophys Res Lett 29(15):1734. doi:10.1029/2002GL015340

Sengupta D, Senan R, Goswami BN, Vialard J (2007) Intraseasonal variability of equatorial Indian Ocean zonal currents. J Clim 20:3036–3055

Sengupta D, Parampil SR, Bhat GS, Murty VSN, Ramesh Babu V, Sudhakar T, Premkumar K, Pradhan Y (2008) Warm pool thermodynamics from the Arabian Sea Monsoon Experiment (ARMEX). J Geophys Res 113:C10008. doi:10.1029/2007JC004623

Shankar D, Vinayachandran PN, Uniikrishnan AS (2002) The monsoon currents in the north Indian Ocean. Prog Ocean 52:63–120

Shenoi SSC, Saji PK, Almeida AM (1999) Near-surface circulation and kinetic energy in the tropical Indian Ocean derived from Lagrangian drifters. J Mar Res 57:885–907

Sikka DR, Gadgil S (1980) On the maximum cloud zone and the ITCZ over the Indian longitudes during the southwest monsoon. Mon Weather Rev 108:1840–1853

Somayajulu YK, Murty VSN, Neelima C, Jagadeesh PSV (2006) Interannual variability of the Equatorial Jets in the Indian Ocean from the merged altimetry data. In: Proceedings of SPIE - The International Society forOptical Engineering, vol 6406, pp 640617-1–640617-11. doi:10.1117/12.693802

Sprintall J, Tomczak M (1992) Evidence of the barrier layer in the surface layer of the tropics. J Geophys Res 97:7305–7316

Thompson B, Gnanaseelan C, Salvekar PS (2006) Variability in the Indian Ocean circulation and salinity and their impact on SST anomalies during dipole events. J Mar Res 64:853–880

Vialard J, Delecluse P (1998a) An OGCM study for the TOGA decade, 1, role of salinity in the physics of the western Pacific fresh pool. J Phys Ocean 28:1071–1088

Vialard J, Delecluse P (1998b) An OGCM study for the TOGA decade, 2, barrier layer formation and variability. J Phys Ocean 28:1089–1106

Vinayachandran PN, Saji NH, Yamagata T (1999) Response of the equatorial Indian Ocean to an unusual wind event during 1994. Geophys Res Lett 26(11):1613–1616

Vinayachandran PN, Iizuka S, Yamagata T (2002) Indian Ocean dipole mode events in an ocean general circulation model. Deep Sea Res II 49:1573–1596

Vinayachandran PN, Francis PA, Rao AS (2009) Indian Ocean dipole: processes and impacts. In: Mukunda N (ed) Current trends in science. Indian Academy of Sciences, India, pp 569–589

Visbeck M, Schott F (1992) Analysis of seasonal current variations in the western equatorial Indian Ocean: direct measurements and GFDL model comparison. J Phys Ocean 22:1122–1128

Webster PJ, Moore A, Loschnigg J, Leban M (1999) Coupled ocean-atmosphere dynamics in the Indian Ocean during 1997–1998. Nature 401:356–360

Webster PJ et al (2002) The JASMINE pilot study. Bull Am Meterol Soc 83:1603–1630

Wentz FJ, Gentemann C, Smith D, Chelton D (2000) Satellite measurements of sea surface temperature through clouds. Science 288:847–850

Wentz FJ, Smith DK, Mears CA, Gentemann CL (2001) Advanced algorithms for QuikSCAT and SeaWinds/AMSR geoscience and remote sensing symposium, *IGARSS* Vol.3, IEEE 2001 International, pp 1079–1081

Wyrtki K (1973) An equatorial jet in the Indian Ocean. Science 181:262–264

Yoshida K (1959) A theory for the Cromwell Current (the Equatorial Undercurrent) and of the equatorial upwelling—an interpretation in a similarity to a coastal circulation. J Oceanogr Soc Jpn 15:159–170

Yu L, O'Brien JJ, Yang J (1991) On the remote forcing of the circulation in the Bay of Bengal. J Geophys Res 96(C11):20449–20454

Yu L, Jin X, Weller RA (2008) Multidecadal global flux datasets from the objectively analyzed air-sea fluxes (OAFlux) project: latent and sensible heat fluxes, ocean evaporation, and related surface meteorological variables. WHOI, OAFlux Project Technical Report, OA-2008-01, 64 pp, Woods Hole, Massachusetts

Yuan D, Han W (2006) Roles of equatorial waves and western boundary reflection in the seasonal circulation of the equatorial Indian Ocean. J Phys Ocean 36:930–944

Zeng X-Z, Li Y-N, Peng S-Q (2012) Analysis of equatorial currents observed by eastern Indian Ocean cruises in 2010 and 2011. Atmos Ocean Sci Lett 5(4):280–283